SEMMELWEIS EGYETEM

DOKTORI ISKOLA

Ph.D. értekezések

2033.

MIRZAHOSSEINI ARASH

A gyógyszerészeti tudományok korszerű kutatási irányai

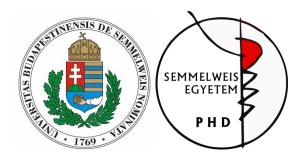című program

Programvezető: Dr. Antal István, egyetemi docens

Témavezető: Dr. Noszál Béla, egyetemi tanár

CHARACTERIZATION OF THIOL-DISULFIDE ACID-BASE AND REDOX EQUILIBRIA WITH SPECIES-SPECIFIC PARAMETERS

PhD thesis

Arash Mirzahosseini

Doctoral School of Pharmaceutical Sciences

Semmelweis University

Supervisor: Béla Noszál, DSc

Official reviewers:
Katalin Ősz, PhD
György Ferenczy, DSc

Head of the Final Examination Committee:
Éva Szökő, DSc

Members of the Final Examination Committee:
Gábor Tóth, DSc
Miklós Csala, DSc

Budapest, 2017

TABLE OF CONTENTS

ABBREVIATIONS

AMARES	advanced method for accurate, robust, and efficient spectral fitting
Boc_2O	di-*tert*-butyl dicarbonate
Calcd	calculated
Cys	cysteine
CysASH	cysteamine
CysASSCysA	cystamine
CysSH	cysteine
CysSSCys	cystine
DHLA	dihydrolipoic acid
DMF	*N,N*-dimethylformamide
DNA	deoxyribonucleic acid
DSS	4,4-dimethyl-4-silapentane-1-sulfonate
Et_3N	triethylamine
$G(OMe)_2SH$	glutathione dimethyl ester
GLRX	glutaredoxin
Glu	glutamate
Gly	glycine
$GOMe_{Gly}SH$	glutathione methyl ester (methylated at the glycinyl residue)
GSH	glutathione

GSSG	glutathione disulfide
hCysSH	homocysteine
HMBC	heteronuclear multiple bond correlation
HPLC	high performance liquid chromatography
HRMS	high resolution mass spectrometry
HSQC	heteronuclear single quantum coherence
MNA$^+$	1-methylnicotinamide
MNAH	1-methyldihydronicotinamide
NAD$^+$	nicotinamide adenine dinucleotide
NADH	dihydronicotinamide adenine dinucleotide
NADP$^+$	nicotinamide adenine dinucleotide phosphate
NADPH	dihydronicotinamide adenine dinucleotide phosphate
NBS	National Bureau of Standards
NMR	nucleic magnetic resonance
Obs	observed
Omm	orders of magnitude minor
OvOMeSSOv	ovothiol A disulfide methyl ester
OvOMeSSOvOMe	ovothiol A disulfide dimethyl ester
OvSH	ovothiol A
OvSHAmide	ovothiol A amide
OvSMe	*S*-methylovothiol A
OvSMeAmide	*S*-methylovothiol A amide

OvSSOv	ovothiol A disulfide
PenSH	penicillamine
PenSSPen	penicillamine disulfide
Ppm	parts per million
Rm	relatively minor
ROS	reactive oxygen species
RSH	thiol
RSSG	glutathione heterodisulfide
RSSR	homodisulfide
SAM	*S*-adenosylmethionine
S.D.	standard deviation
TFA	trifluoroacetic acid
TOFMS	time-of-flight mass spectrometry
UV	ultraviolet
UV/VIS	ultraviolet/visible light

1. INTRODUCTION

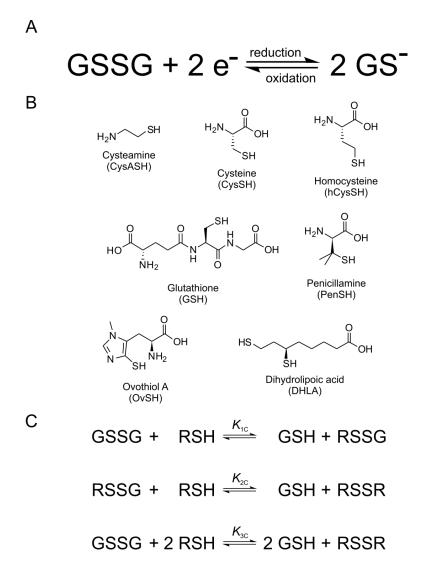## 1.1 Redox homeostasis and oxidative stress

It is through the decomposition of intricate biophysical chemical networks into elementary steps that the underlying mechanisms of (patho)biochemical processes can be well understood. The underlying fundamental reactions of metabolism, redox reactions, form reactive oxygen species (ROS) amid the natural respiration of every organism. Due to their highly reactive nature, these species are difficult to observe and therefore the knowledge regarding their biochemistry is hitherto developing. It is understood that these species play a key role in vital cellular regulation mechanisms, such as proliferation, cellular motility, transcription, transport, membrane integrity, immune responses, and programmed cell death [1]. The amount of ROS is regulated by a powerful antioxidant defense system within the cells to minimize their damage. The imbalance between the prooxidant and antioxidant pathways in the favor of the former however, may lead to oxidative stress. Prolonged oxidative damage exerted on DNA, membrane lipids, proteins, or the mitochondria has a pivotal role in the pathogenesis of various diseases, such as cancer, neurodegeneration (multiple sclerosis, Alzheimer's disease, Parkinson's disease, amyotrophic lateral sclerosis), cardiovascular diseases (atherosclerosis, cardiac ischemia, reperfusion), and pulmonary diseases (cystic fibrosis) to name a few [1]. The intracellular redox homeostasis is maintained mainly by oxidoreductase enzymes of the antioxidant system. The redox reactions occurring in biochemical processes, while diverse in character, are one- or two-electron transitions primarily taking the form of thiol-disulfide exchange. In fact, the thiol-disulfide pool is thought to be chiefly responsible for the intracellular redox homeostasis [2]. Enzymes play an undeniable role in governing these biochemical processes. However, it is vital that the characteristics, fine tuning, and optimization of non-enzymatic, 'small molecule' antioxidants are also understood, since the despondent fight against oxidative stress is in critical need of a potent antioxidant drug; an urgent unmet therapeutic need worldwide.

7

1.2 Thiol chemistry

The uptake and metabolism of sulfur is a *sine qua non* process for life. The eminent peptide- and protein-building sulfur-containing biomolecules are cysteine (CysSH) and methionine. However, numerous other biochemical processes owe their *raison d'être* to the intriguing chemistry of sulfur [3]. For instance, the high-energy thioester bond in acetyl (or malonyl) coenzyme A, assembled from the decarboxylated derivative of cysteine (cysteamine, CysASH), serves as the basis for the junction of almost all of eukaryote biometabolism. Iron-sulfur clusters [4] and sulfur oxygenation reactions [5] are the initiators of radical chemistry. Methyltransferase and transsulfuration reactions, crucial for nucleic acid and protein production, make also use of *S*-adenosylmethionine (SAM) cycles [6]. One of the secondary metabolites of methionine metabolism is homocysteine (hCysSH), a candid risk factor of cardiovascular diseases [7-8]. Direct thiol-disulfide interchange is often the rate limiting step in protein folding processes.

The thiol-containing biomolecules in the redox homeostasis and signal transduction of cells bear highly promising therapeutic capacity [9-10]. Acting as a ubiquitous antioxidant, glutathione (γ-L-glutamyl-L-cysteinylglycine, GSH) protects cell organelles from reactive oxygen species, precluding thus neurodegenerative, cardiovascular and neoplastic pathobiochemical processes [11-12]. Nevertheless, an efficacious antioxidant or a set of selective antioxidants are urgent medical needs. In order to achieve these goals, a thorough understanding of thiol-disulfide equilibria is certainly required. Glutathione is the single most important non-enzymatic intracellular antioxidant. As the prime molecule of the physiological defense system against reactive oxygen species, the agents of oxidative stress, GSH is oxidized to glutathione-disulfide (GSSG) as seen in Figure 1. Glutathione is a key factor in the maintenance of the redox homeostasis of biological systems, due partly to its cellular concentration exceeding that of other antioxidants. The concentration of GSH ranges between 0.5 and 10 mmol/L [13], and is largely maintained in its reduced form by glutathione reductase [14-15]. Glutathione is also responsible for the regulation of the thiol-disulfide balance in proteins and biogenic thiols [16-17]. In addition to its major role in oxidative stress and related pathophysiological conditions [18], glutathione is also the preeminent means of detoxification [19]. The ubiquitous and effective GSH-GSSG redox system is the most

thoroughly studied one [20], does not require enzyme catalysis to function, can be applied in aqueous media under a wide range of conditions. These advantages make the GSH-GSSG system a "gold standard" in thiol-disulfide biochemistry; hence every thiol-containing antioxidant is compared to glutathione [16]. The acid-base properties of GSH have long been in the focus of scientific interest [21-24], and even the species-specific protonation constants of GSH [25] and GSSG [26] have been studied. Nevertheless, these values are only those of the major pathways.

A

$$GSSG + 2\ e^- \underset{\text{oxidation}}{\overset{\text{reduction}}{\rightleftharpoons}} 2\ GS^-$$

B

Cysteamine (CysASH)

Cysteine (CysSH)

Homocysteine (hCysSH)

Glutathione (GSH)

Penicillamine (PenSH)

Ovothiol A (OvSH)

Dihydrolipoic acid (DHLA)

C

$$GSSG + RSH \overset{K_{1C}}{\rightleftharpoons} GSH + RSSG$$

$$RSSG + RSH \overset{K_{2C}}{\rightleftharpoons} GSH + RSSR$$

$$GSSG + 2\ RSH \overset{K_{3C}}{\rightleftharpoons} 2\ GSH + RSSR$$

Figure 1. A: The thiol-disulfide redox half-reaction of glutathione. B: The structural formulae of the thiols studied. C: Scheme of the thiol-disulfide equilibria at the macroscopic level. RSH denotes the thiols; RSSR denotes their respective homodisulfides; RSSG denotes their respective heterodisulfides formed with glutathione.

It is a key feature of any thiol-disulfide redox system, that only the deprotonated thiol species are active in the redox process, i.e. only the anionic thiolate can be oxidized directly [27-30]. Since the deprotonated fraction of thiols depends on the solution pH, the oxidation-reduction potential of thiol-containing biomolecules is also pH-dependent. These interwoven acid-base and redox processes are usually further influenced by overlapping protonation processes of multiple basic centers on the molecule in question. Therefore, the redox potential of thiol-containing biomolecules is usually doubly pH-dependent. Primarily, the deprotonated fraction of every thiol depends on the pH of the solution, with strong dependence typically in the 6-11 pH range [16]. One clear exception to this typical acid-base behavior is ovothiol A with extremely low thiolate basicities [31], which extends the general basicity range for thiolates to 1-10 log units in terms of protonation constants. Secondarily, the thiolate oxidizability in most biomolecules is modulated by the adjacent basic groups, since protonation of any such group exerts an electron-withdrawing effect on the thiolate. In a molecule of $n+1$ basic sites the thiolate has 2^n different, distinct oxidizabilities within a single, covalently unchanged molecular skeleton. Thus, macroscopic physico-chemical parameters cannot quantify the thiolate moiety specifically. A thorough characterization of the thiol-disulfide equilibria can be achieved by means of species-specific, so-called microscopic parameters, which are, in fact, well-established terms for acid-base systems [32-33].

Ovothiol A (($2S$)-2-amino-3-(3-methyl-5-sulfanylimidazol-4-yl)propanoic acid, OvSH) is a naturally occurring 4-mercaptohistidine derivative [34-36] first observed in sea urchin (*Strongylocentrotus purpuratus*) eggs by Turner *et al.* [37]. Ovothiol A (henceforth referred to as simply ovothiol), B, and C differ in the level of methylation at the amino site: latters are mono- and dimethyl derivatives, respectively. Mercaptohistidines also exist in marine algae [38], trout and salmon eggs [39] and related aquatic organisms. The function of ovothiols in marine invertebrate eggs is hypothesized to be defense against oxidative stress agents [39-40]. Ovothiol along with novel mercaptohistidines has been detected in many parasitic protozoa [41-45]. The molecular structure of ovothiol is certainly unique among naturally occurring small molecules: the number and especially the variety of functional groups relative to its low molecular mass greatly exceeds those of almost all other biomolecules. The uncommon positioning of the thiol group results in peculiar acid-base properties: the thiolate group

has an extremely low basicity [31,46]. The interaction between the imidazole ring and the thiol group also results in the significant elevation of the imidazole basicity compared to that of histidine. The observation that thiolate basicities and thiol-disulfide half-cell redox potentials are in correlation [16] supports the hypothesis [47-50] that ovothiol is one of the most potent natural antioxidants even in low pH media. The many interesting features of this molecule have prompted studies to find candidates for drug development. A new prospect has emerged in search of a non-synthetic antioxidant [51-52], anticipating results in neurodegenerative therapy [53]. A different approach exploits the biological role of ovothiols to create prospective antitrypanosomal chemotherapeutic agents [54-55] by inhibiting the biosynthetic enzymes; since the synthesis of ovothiols and trypanothiones (not present in host cells) is essential for the survival of trypanosomatids.

The direct measurement of the redox potential for thiol-disulfide systems, by usual electrochemical methods is not feasible due to formation of stable metal-thiolate complexes at electrode surfaces [56]. Thus the redox potentials of GSH and other thiols can only be determined indirectly by measurement of equilibrium constants for their reaction with redox systems of known redox potentials [20]. However, until now only the apparent redox potential of GSH was determined, largely because the highly composite species-specific acid-base properties, which are in codependent interference with the redox behavior, were not known. The general scheme of thiol-disulfide redox equilibria (as depicted in Figure 1) is generally studied at the level of phenomena; the three conditional equilibrium constants are expressed by equations (1)-(3) and the Nernstian redox potential of a thiol-disulfide redox couple are expressed by equation (4).

$$K_{1C} = \frac{[GSH][RSSG]}{[RSH][GSSG]} \tag{1}$$

$$K_{2C} = \frac{[GSH][RSSR]}{[RSH][RSSG]} \tag{2}$$

$$K_{3C} = K_{1C}K_{2C} = \frac{[\text{GSH}]^2[\text{RSSR}]}{[\text{RSH}]^2[\text{GSSG}]} \qquad (3)$$

$$E = E° + \frac{RT}{zF}\ln\frac{[\text{RSSR}]}{[\text{RSH}]^2} \qquad (4)$$

1.3 Species-specific chemical microequilibria

Figures 2, 3 and 4 represent the species-specific protonation scheme of a bidentate thiol (cysteamine) and its homodisulfide, a tridentate thiol (cysteine, homocysteine, penicillamine) and its homodisulfide, and a tetradentate thiol (glutathione, ovothiol) and its homodisulfide, respectively. Macroequilibria (top lines) indicate the stoichiometry of the successively protonated ligand and the stepwise macroscopic protonation constants. In the microspeciation schemes, the different microspecies with their one-letter symbols (a, b, c …), and the microscopic protonation constants are depicted (k^N, k_N^S …). The superscript at k for any microconstant indicates the protonating group while the subscript (if any) shows the site(s) already protonated. S, N, O, G and E symbolize the thiolate, amino, carboxylate (in cysteine and cystine), glycinyl carboxylate and glutamyl carboxylate (in GSH and GSSG after their one-letter symbol) sites, respectively. Some protonation constant examples for cysteine are shown below:
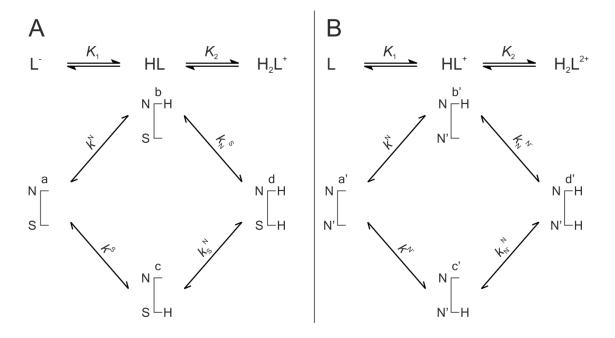
$$K_2 = \frac{[\text{H}_2\text{L}]}{[\text{HL}^-][\text{H}^+]} \qquad (5)$$

$$\beta_3 = K_1K_2K_3 = \frac{[\text{H}_3\text{L}^+]}{[\text{L}^{2-}][\text{H}^+]^3} \qquad (6)$$

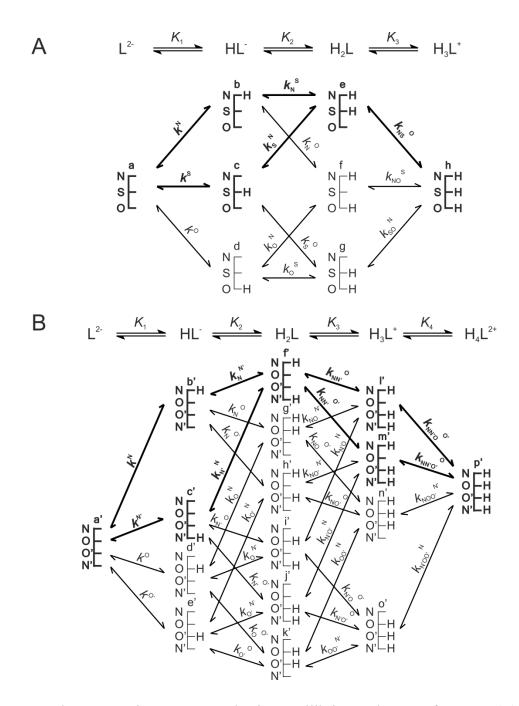$$k^N = \frac{[\text{b}]}{[\text{a}][\text{H}^+]} \qquad (7)$$

where K_1, K_2, K_3, are successive macroconstants, β_3 is one of the cumulative macroconstants, k^N is the microconstant of cysteine involved in the production of

microspecies b. The concentrations of the various macrospecies comprise the sum of the concentration of those microspecies that contain the same number of protons, for example in GSH:
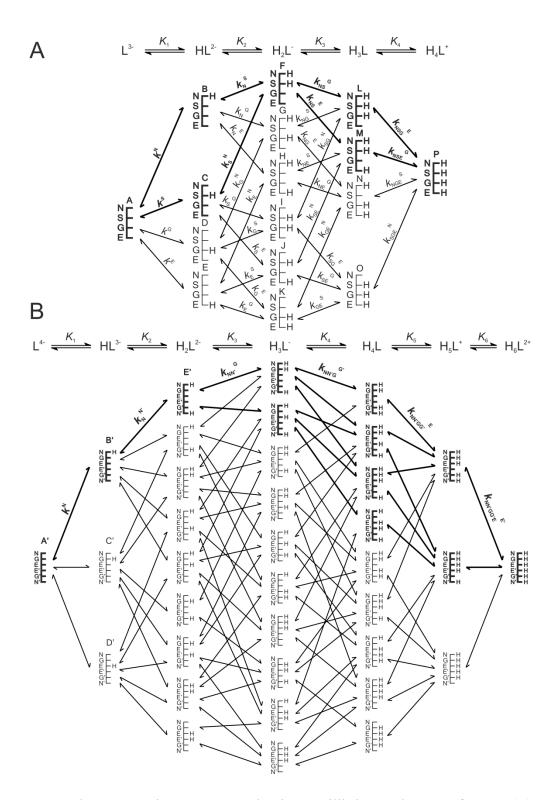
$$[H_2L^-] = [F] + [G] + [H] + [I] + [J] + [K] \tag{8}$$

Figure 2. The protonation macro- and microequilibrium schemes of CysASH (A) and CysASSCysA (B) in terms of stepwise macroscopic protonation constants (K_1, K_2), where L$^-$, HL, etc. are the successively protonating ligands (top lines). Below are the species-specific protonation schemes in terms of microspecies (a, b, c, d) and microscopic protonation constants (k^N, k_N^S …).

Figure 3. The protonation macro- and microequilibrium schemes of CysSH (A) and CysSSCys (B) in terms of stepwise macroscopic protonation constants (K_1, K_2, K_3 …), where L^{2-}, HL^-, etc. are the successively protonating ligands (top lines). Below are the species-specific protonation schemes in terms of microspecies (a, b, c …) and microscopic protonation constants (k^N, k_N^S …). The components of the major pathways are in bold. The above schemes are also representative of the other tridentate thiols, i.e. homocysteine and penicillamine.

Figure 4. The protonation macro- and microequilibrium schemes of GSH (A) and GSSG (B) in terms of stepwise macroscopic protonation constants (K_1, K_2, K_3 …), where L^{3-}, HL^{2-}, etc. are the successively protonating ligands (top lines). Below are the species-specific protonation schemes in terms of microspecies (A, B, C …) and microscopic protonation constants (k^N, k_N^S …). For GSSG, only non-identical

microspecies and microconstants are shown, and only a few of the microconstants are depicted. The components of the major pathways are in bold. The protonation schemes of OvSH and OvSSOv are identical to the depicted schemes except Im (imidazole) and O (carboxylate) moieties are present instead of G and E.

The relationships between the macro- and microconstants defined first in the pioneer work of Niels Bjerrum [32] can be applied to cysteine:

$$\beta_1 = k^N + k^S + k^O \tag{9}$$

$$\beta_2 = k^N k_N^S + k^N k_N^O + k^S k_S^O = \dots \tag{10}$$

$$\beta_3 = k^N k_N^S k_{SN}^O = \dots \tag{11}$$

Depending on the path of protonation, equations (10) and (11) can be written in 2 and 6 different, equivalent ways, respectively. Determination of protonation microconstants needs careful considerations and has been elaborated in detailed in a recent review [33]. The characterization of the microspeciation scheme necessitates the knowledge of the macroscopic protonation constants (accessible from titrimetric measurements) and the utilization of a species-specific spectroscopic assay or the introduction of auxiliary model compounds. The application of a spectroscopic method that delivers selective information regarding one or some of the basic sites in the molecule in question can in principle allow the determination of all microconstants. However, with decreasing size and an omni-interactive molecular skeleton the probability that a selective analyte signal can be found diminishes rapidly. Minor microspecies influence the analytical signals (NMR, UV, etc.) insignificantly, but they may be the reactive species in highly specific biochemical processes [57]. An alternative method for the elucidation of protonation microconstants is the deductive method; by way of this method model compounds are synthesized that are the closest possible mimics of the minor microspecies. The protonation constants of the simpler model compounds are regarded as constituent

elements of the microspeciation scheme. For the case of thiols, the model compounds were synthesized by methylating the thiol and carboxyl groups, thereby modeling the protonated form of these moieties. The site in which the methyl group is connected remains in neutral state, with practically identical electronic effects on the rest of the molecule as –COOH and –SH groups [58-59]. Using analogous equations as equations (9) and (11), and by introducing interactivity parameters, the calculation of leftover microconstants becomes straightforward. The interactivity parameter shows to what extent the protonation of site A reduces the basicity of site B, and vice versa. The interactivity parameter is generally considered to be the most invariant quantity in analogous moieties of different compounds and also in various protonation states of the neighboring moiety in the same molecule [60].

For the thiol-disulfide redox equilibria, only the apparent or conditional equilibrium constants (K_{3C}) are directly available, by determining the equilibrium concentrations of RSH, GSSG, RSSR, and GSH in the reaction mixtures. In other words: these conditional equilibrium constants are pH-dependent parameters in terms of total concentrations of the thiol and disulfide species that are present, since the spectroscopic intensity of the analyte signal corresponds to the total concentration of a thiol reactant that is actually composed of the concentration of the variously protonated microspecies. The concentration of the macrospecies can be written as the sum of the microspecies of the same number of bound protons, as shown in equation (8) for H_2L^- of GSH. The pH-dependent, apparent constants can be decomposed into pH-independent, species-specific equilibrium constants, the number of which is large, but definite. For example, the thiolate moiety in cysteine is adjacent to two other basic sites; the amino and the carboxylate groups. Therefore, the thiolate-bearing microspecies can exist in 4 different protonation states. Concurrently, the thiolates in the 4 different microspecies will be in different electrostatic environments, thus having 4 different oxidizabilities. Considering the opposite direction of the redox equilibrium, GSH with an amino and two carboxylate sites can have 8 different thiolate-bearing microspecies with 8 different electron densities on its sulfur. This leads to 4x8=32 different microscopic redox equilibria between cysteine and glutathione.

Since redox and acid-base reactions coexist, the observed apparent redox equilibrium constants, K_{1C}, K_{2C}, and K_{3C} are pH-dependent. In order to get a clear insight into the redox equilibria, purified from the protonation effects, an improved evaluation method had to be introduced, including a set of species-specific, new type of redox equilibrium constants (k_1, k_2, k_3). As equation (3) shows the complete redox transition includes two thiols and two disulfides. We therefore confined our efforts to the determination of the K_{3C} macroconstants, and the related k_3 microconstants, the number of which can certainly be numerous. This confinement overcomes the highly complex quantification of the heterodisulfides, which actually improves perspicuity. Keire *et al.* [16] have already demonstrated that a) there is correlation between the thiolate basicities and redox properties and b) purely redox thiol-disulfide equilibrium constants can only be obtained if these transitions can be decoupled from the acid-base processes by an appropriate evaluation method. Determination of the redox equilibrium constants requires all the species-specific protonation constants, including those of the minor microspecies; otherwise, redox processes could only be characterized at the level of phenomenon, especially for acidic media.

To epitomize the determination of microscopic redox equilibrium constants (k_3) from the conditional equilibrium constants (K_{3C}), the calculation of the k_3^{bB} for the reaction involving the b microspecies of cysteine, the corresponding f' cystine microspecies, the B glutathione microspecies, and the corresponding E' glutathione disulfide microspecies will be demonstrated. Note that b and B define that the disulfide microspecies are f' and E', since these are the only ones with identical protonation states in the side-chain. Superscripts b and B therefore unambiguously identify all the 4 microspecies in the microequilibrium in question. This example of the pH-independent, microscopic thiol-disulfide equilibrium constants is expressed by equation (12):

$$k_3^{bB} = \frac{[B]^2[f']}{[b]^2[E']} \tag{12}$$

Quantification of redox equilibria in terms of such pH-independent, species-specific constants has long been a conceptual endeavor. The obvious reason why it has not so far been achieved is the fact that the microspecies concentrations cannot be measured. As shown below, the species-specific constants can be, however, obtained as the product of total species concentration and the relative abundance of the respective microspecies. The relative abundance of the microspecies in turn, is a function of pH and the microscopic protonation constants. For the b cysteine microspecies, the concentration can be written as follows:

$$[b] = [CysSH]\chi_b = [CysSH]\frac{k^N[H^+]}{1 + \beta_1^{CysSH}[H^+] + \beta_2^{CysSH}[H^+]^2 + \beta_3^{CysSH}[H^+]^3} \qquad (13)$$

where [CysSH] is the total solution concentration of cysteine, x_b is the relative abundance of microspecies b (i.e. x_b = [b]/[CysSH]), k^N is the microscopic protonation constant of cysteine involved in the formation of microspecies b. Substituting analogous equations as equation (13) for the concentrations of the microspecies in k_3^{bB}, one can write the equation of the microscopic equilibrium constant as follows:

$$k_3^{bB} = \frac{[B]^2[f]}{[b]^2[E']} = \frac{[GSH]^2\chi_B^2[CysSSCys]\chi_f}{[CysSH]^2\chi_b^2[GSSG]\chi_{E'}} = K_{3C}\frac{\chi_B^2\chi_f}{\chi_b^2\chi_{E'}} \qquad (14)$$

Thus, if K_{3C}, the apparent equilibrium constant and the 4 x values (as functions of the protonation constants and pH) have previously been determined, the k_3^{bB} value and all the analogous, pH-independent, species-specific redox microconstants can be calculated.

19

2. OBJECTIVES

The objectives of the doctoral thesis are the following:

- determination of the species-specific protonation constants of the most important biological thiols and their homodisulfides, namely: cysteamine, cysteine, homocysteine, penicillamine, glutathione, ovothiol, dihydrolipoic acid;
- determination of the species-specific redox equilibrium constants of the thiol-disulfude interchange reactions respective to glutathione;
- determination of the species-specific standard redox potential of glutathione using an indirect redox system for comparison, namely: 1-methylnicotinamide;
- determination of the species-specific standard redox potential of the most important biological thiols.

3. METHODS

3.1 Materials

All chemicals used for analytical and synthetic purposes were purchased from Sigma-Aldrich (Saint Louis, MO, USA) and used without further purification. Ovothiol and every model compound were synthesized according to the synthetic protocols described in section 3.9.

3.2 NMR spectroscopy measurements

NMR spectra were recorded on a Varian 600 MHz spectrometer at 298.2 ±0.1 K. The solvent in every case was an aqueous solution with $H_2O:D_2O$, 95:5, v/v (0.15 mol/L ionic strength), using DSS sodium (4,4-dimethyl-4-silapentane-1-sulfonate) as the reference compound. The sample volume was 600 μL, pH values were determined by internal indicator molecules optimized for NMR [61-62]. ^{1}H NMR spectra were recorded with the presaturation solvent suppression sequence (number of transients=64, number of points=16384, acquisition time=851.968 ms, relaxation delay=15 s). For the ^{15}N NMR measurements WET-HMBC sequence was used, with tetraethylammonium chloride (20 mmol/L, -316.7 ppm [63]) as a nitrogen standard. The solutions used to determine the protonation constants of the thiols also contained dithiothreitol to preclude oxidation.

3.3 pH-potentiometric titrations

A 716 DMS Titrino automatic titrator (Metrohm AG, Herisau, Switzerland) with a Metrohm 6.0204.100 combined pH glass electrode was used for the pH-potentiometric titrations, under automatic PC control. The electrode was calibrated by aqueous NBS standard buffer solutions. Constant temperature (298.2 ±0.1 K) was provided by a thermostated double-walled glass cell. Difference titrations were carried out in the absence (blank) and presence of ligands. First 1.5 mL of 0.1 mol/L HCl solutions were

titrated with 0.1 mol/L NaOH. Constant ionic strength of 0.15 mol/L was provided by the presence of KCl. Next, a ligand was added to the same volume of HCl solution and was subsequently titrated with NaOH. The initial concentration of the ligand was around 5 mmol/L in the titrations. Non-linear parameter fitting with Origin Pro 8 (OriginLab Corp., Northampton, MA, USA) provided the protonation constants from the interpolated volume differences.

3.4 UV spectroscopy measurements

Absorbance data were recorded on a Jasco V-550 UV/VIS spectrophotometer (serial-no: C02951185, Jasco Intl. Co. Ltd., Tokyo, Japan). pH values were read on Metrohm 2.780.0010 precision pH meter with a 6.0258.600 Unitrode glass Pt 1000 electrode (Metrohm AG, Herisau, Switzerland), the pH-potentiometric system was calibrated using pH 1.68, 4.01, 6.87, 9.18 aqueous NBS standard buffer solutions. The samples were prepared by mixing an acidic and basic solution of the titrand (adjusted with HCl and NaOH, 0.15 mol/L ionic strength) in different ratios, the reference solution for the UV measurements was an aqueous solution adjusted to the same pH as the sample with HCl and NaOH.

3.5 Electrochemical measurements

The redox electrode (Radeklis OP-6123, Radeklis, Budapest, surface area ~2 cm^2) used for electrode potential measurements was washed with 50 % nitric acid, then distilled water before each measurement and gently dried by touching onto tissue paper. The redox electrode was calibrated using ZoBell's solution (2.64 g K$_4$[Fe(CN)$_6$].3H$_2$O and 2.06 g K$_3$[Fe(CN)$_6$].H$_2$O dissolved in 500 mL pH=7 0.15 mol/L Na$_2$HPO$_4$/KH$_2$PO$_4$ buffer). The electrode potential measurements were carried out using a Radelkis Laboratory Digital pH/mV meter OP-211/2 (Radelkis, Budapest) at 298 ±2 K in an 815-PGB glove box (Plas-Labs Ic., Lansing, MI, USA) under N$_2$ atmosphere to preclude oxidation by air. All potentials were referred to saturated calomel electrode as reference

electrode. The pH values of the samples were determined using a Metrohm 6.0204.100 combined pH glass electrode, calibrated by aqueous NBS standard buffer solutions.

3.6 Preparation of solutions for equilibrium constant determination

Acidic (pH=0.85) and basic (pH=13.15) stock solutions containing the reagents were prepared in an 815-PGB glove box (Plas-Labs Ic., Lansing, MI, USA) under N_2 atmosphere to preclude oxidation by air. The concentrations of the reagents were optimized for quantitative NMR, ca. 15 mmol/L. A series of solutions with different pH values were prepared by mixing the acidic with the basic stock solutions. D_2O, DSS, glutathione reductase, and a pH indicator, which also served as a concentration standard, were added to the solutions. The samples were protected from sunlight and kept in the glove box under N_2 atmosphere (298 ±2 K) for at most 7 days, until the reactions in all the samples had reached equilibrium.
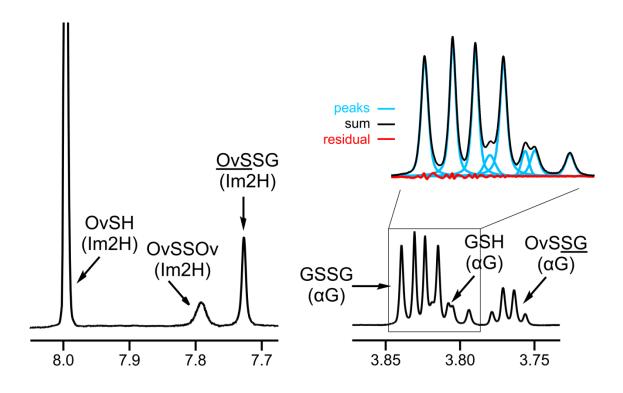
3.7 Mathematical analysis

For the analysis of NMR titration curves of proton chemical shifts versus pH, the software Origin Pro 8 (OriginLab Corp., Northampton, MA, USA) was used. In ^{1}H NMR-pH and potentiometric titrations the non-linear curve fitting regression analysis option was used with the following functions [64], respectively:

$$\delta_{obs}(pH) = \frac{\sum_{i=0}^{n} \delta_{H_iL} 10^{\log \beta_i - ipH}}{\sum_{i=0}^{n} 10^{\log \beta_i - ipH}} \qquad (15)$$

$$\Delta V(pH) = A \frac{\sum_{i=0}^{n} i 10^{\log \beta_i - ipH}}{\sum_{i=0}^{n} 10^{\log \beta_i - ipH}} + D \qquad (16)$$

where δ_{H_iL} values stand for the chemical shifts of successively protonated ligands, n is the maximum number of protons that can bind to L, β is the cumulative protonation macroconstant, A is the NaOH volume corresponding to one unit of deprotonation, and D is the experimental correction fitting factor. The standard deviations of $\log\beta$ values from the regression analyses were used to calculate the Gaussian propagation of uncertainty to the protonation microconstants derived in the Results chapter.

For the analysis of quantitative NMR measurements (sample spectrum in Figure 5), the AMARES [65] time domain fit algorithm (without apodization) of the jMRUI v. 5.1 software package [66] was used. For the regression analyses, the software Origin Pro 8 (OriginLab Corp., Northampton, MA, USA) was used. The standard deviations of the peak areas obtained by fitting Lorentzian peak shapes, the error of pH determination, and the standard errors of the microscopic redox equilibrium constants were used to calculate the Gaussian propagation of uncertainty to the standard redox potentials derived in the Results chapter.

Figure 5. The expanded ^{1}H NMR spectrum of a sample containing ovothiol-glutathione mixture with example of peak fitting result (pH=9.20).

3.8 TOF MS measurements

The exact mass of the synthesized and isolated compounds was determined with an Agilent 6230 time-of-flight mass spectrometer equipped with a JetStream electrospray ion source in positive ion mode. JetStream parameters: drying gas (N_2) flow and temperature: 10.0 L/min and 598 K; nebulizer gas (N_2) pressure: 10 psi; capillary voltage: 4000 V; sheath gas flow and temperature: 598 K and 7.5 L/min. TOFMS parameters: fragmentor voltage: 170 V; skimmer potential: 170 V; OCT 1 RF Vpp: 750 V. Samples were introduced (0.1-0.3 µL) by the Agilent 1260 Infinity HPLC system (flow rate=0.5 mL/min, 70% methanol-water mixture 0.1% formic acid). Reference masses of *m/z* 121.050873 and 922.009798 were used to calibrate the mass axis during analysis. Mass spectra were acquired over the *m/z* range 100-1000 at an acquisition rate of 250 ms/spectrum and processed using Agilent MassHunter B.02.00 software.

3.9 Synthetic protocols

3.9.1 Synthesis of ovothiol

The total synthesis of ovothiol has been reported [67] and remains the preferred method of preparation, compared to the cumbersome task of gathering sea urchin eggs for extraction [37]. However the total synthesis reported by Holler *et al.* contains 9 steps, constructing the imidazole ring from scratch and has a total yield of 11%. A simpler method was therefore exploited, making use of histidine as the natural precursor to synthesize ovothiol in an enantiopure, convenient and cost-effective way (Figure 6). The configuration of the end-product was verified with optical rotatory dispersion measurement of ovothiol disulfide.

Figure 6. The synthesis route of ovothiol.

(2S)-2-[(*tert*-Butoxycarbonyl)amino]-3-[1-(*tert*-butoxycarbonyl)-1H-imidazol-4-yl]-propanoic acid (2). To a suspension of L-histidine (**1**) (1.43 g, 9.2 mmol) in methanol (CH$_3$OH) (30 mL), 3.24 g (21.2 mmol) of di-*tert*-butyl dicarbonate (Boc$_2$O) and 1.8 mL (18.4 mmol) of triethylamine (Et$_3$N) were added. The reaction mixture was stirred at room temperature overnight. The reaction mixture was then concentrated under vacuum and the crude product was purified on silica gel with column chromatography (CHCl$_3$:CH$_3$OH 9:1) to give 3.01 g (yield 92%) white solid: mp 346-348 K [68] (from chloroform, CHCl$_3$); ^{1}H NMR (600 MHz, DMSO-d_6) δ 1.40 (9H, s, N$^{\alpha}$CO$_2$C(CH$_3$)$_3$), 1.61 (9H, s, N$^{\text{Im}}$CO$_2$C(CH$_3$)$_3$), 2.87 (1H, dd, J 8, 15 Hz, βH), 3.08 (1H, dd, J 4, 15 Hz, βH), 4.25 (1H, dd, J 4, 8 Hz, αH), 7.29 (1H, s, Im^{5}H), 8.06 (1H, s, Im^{2}H); ^{13}C NMR (600 MHz, CD$_3$OD) δ 28.1 (N$^{\alpha}$Boc-CH$_3$), 28.8 (N$^{\text{Im}}$Boc-CH$_3$), 31.1 (βC), 56.6 (αC), 80.1 (N$^{\alpha}$Boc-t-C), 86.9 (N$^{\text{Im}}$Boc-t-C), 116.1 (Im^{4}C), 137.6 (Im^{5}C), 141.1 (Im^{2}C), 148.3 (N$^{\alpha}$Boc-C=O), 157.5 (N$^{\text{Im}}$Boc-C=O), 178.1 (COOH); HRMS *m/z* [M+H]$^+$ Calcd: 356.1822, Found: 356.1824.

Methyl (2S)-2-[(*tert*-butoxycarbonyl)amino]-3-(1-methyl-1H-imidazol-5-yl)propanoate (3). To the solution of (**2**) (3.01 g, 8.5 mmol) in 20 mL CH$_3$OH, 1.32

mL (21.3 mmol) of iodomethane (CH_3I) was added at 273 K. The solution mixture was stirred overnight at 273 K. The reaction mixture was then extracted with ethyl acetate (after adjusting the pH between 7 and 8) and washed with brine. The resulting organic layer was dried over anhydrous sodium sulfate and concentrated under vacuum. The crude product was purified on silica gel with column chromatography (ethyl acetate:acetone 9:1) to give 1.97 g (yield 83%) white solid (the position of the methyl group on the imidazole ring was confirmed using NOESY [69] and ^{1}H-^{15}N HMBC [70]): mp 382-383 K (from ethyl acetate); ^{1}H NMR (600 MHz, CD_3OD) δ 1.40 (9H, s, $CO_2C(CH_3)_3$), 2.98 (1H, dd, J 9, 15 Hz, βH), 3.14 (1H, dd, J 5, 15 Hz, βH), 3.66 (3H, s, NCH_3), 3.74 (3H, s, OCH_3), 4.42 (1H, dd, J 5, 9 Hz, αH), 6.78 (1H, s, Im^5H), 7.59 (1H, s, Im^2H); ^{13}C NMR (600 MHz, CD_3OD) δ 27.1 (βC), 28.7 (Boc-CH_3), 31.8 (NCH_3), 52.9 (OCH_3), 54.2 (αC), 80.8 (Boc-t-C), 127.5 (Im^5C), 129.4 (Im^4C), 139.2 (Im^2C), 157.7 (Boc-C=O), 173.4 (COO); HRMS m/z [M+H]$^+$ Calcd: 284.1610, Found: 284.1602.

Methyl (2S)-3-(4-bromo-1-methyl-1H-imidazol-5-yl)-2-[(tert-butoxycarbonyl)amino]-propanoate (4). To the solution of (**3**) (1.02 g, 3.6 mmol) in 10 mL CH_3OH, 0.71 g (4.0 mmol) of N-bromosuccinimide (NBS) was added in small amounts at 273 K. The reaction mixture was stirred at 273 K for 2 hours, and then the reaction mixture was concentrated under vacuum. The crude product was purified on silica gel with column chromatography (ethyl acetate:$CHCl_3$ 9:1) to give 0.98 g (yield 75%) white glassy solid: ^{1}H NMR (600 MHz, CD_3OD) δ 1.38 (9H, s, $CO_2C(CH_3)_3$), 2.99 (1H, dd, J 9, 15 Hz, βH), 3.15 (1H, dd, J 6, 15 Hz, βH), 3.69 (3H, s, NCH_3), 3.73 (3H, s, OCH_3), 4.40 (1H, t, J 7 Hz, αH), 7.55 (1H, s, Im^2H); ^{13}C NMR (600 MHz, CD_3OD) δ 27.1 (Boc-CH_3), 28.6 (βC), 33.0 (NCH_3), 49.8 (OCH_3), 53.7 (αC), 79.4 (Boc-t-C), 115.5 (Im^5C), 126.8 (Im^4C), 138.9 (Im^2C), 157.4 (Boc-C=O), 181.5 (COO); HRMS m/z [M+H]$^+$ Calcd: 362.0715, Found: 362.0720.

(2S)-2-[(tert-Butoxycarbonyl)amino]-3-{1-methyl-4-[(4-methylbenzyl)sulfanyl]-1H-imidazol-5-yl}propanoic acid (5). A solution of (**4**) (0.98 g, 2.7 mmol) and 1 mL (8.1 mmol) of (4-tolyl)methanethiol in 10 mL dry N,N-dimethylformamide (DMF) was added dropwise in nitrogen (N_2) atmosphere to a stirred solution of 98 mg (4.1 mmol) sodium hydride (NaH) in 10 mL dry DMF. The reaction mixture was heated at 393 K in

an atmosphere of N_2 for 3 hours. After cooling, the reaction mixture was concentrated *in vacuo* to leave a brown oil. The crude product was purified on silica gel with column chromatography (CH_2Cl_2:n-hexane 2:1) to give 0.81 g (yield 74%) brown oil: ^{1}H NMR (600 MHz, CD_3OD) δ 1.31 (9H, s, $CO_2C(CH_3)_3$), 2.27 (3H, s, $ArCH_3$), 2.63 (1H, dd, *J* 10, 15 Hz, βH), 2.82 (1H, dd, *J* 4, 15 Hz, βH), 3.67 (3H, s, NCH_3), 3.81 (1H, d, *J* 13 Hz, SCH_2), 3.86 (1H, d, *J* 13 Hz, SCH_2), 4.09 (1H, dd, *J* 4, 10 Hz, αH), 6.97 (2H, d, *J* 8 Hz, o-ArH), 7,00 (2H, d, *J* 8 Hz, m-ArH), 7.56 (1H, s, Im^2H); ^{13}C NMR (600 MHz, CD_3OD) δ 21.1 ($ArCH_3$), 28.7 (Boc-CH_3), 31.1 (βC), 32.7 (NCH_3), 41.2 (SCH_2), 55.9 (αC), 79.5 (Boc-*t*-C), 129.7 (o-Ar), 129.8 (Im^5C), 129.9 (m-Ar), 134.5 (p-Ar), 137.5 (i-Ar), 139.3 (Im^4C), 156.9 (Im^2C), 161.4 (Boc-C=O), 178.0 (COOH); HRMS m/z [M+H][+] Calcd: 406.1800, Found: 406.1794.

(2*S*)-2-Amino-3-(1-methyl-4-sulfanyl-1*H*-imidazol-5-yl)propanoic acid, ovothiol (6). 82 mg (0.2 mmol) of (**5**) was dissolved in 0.5 mL anisole and cooled to 273 K. Mercury(II) trifluoroacetate, 173 mg (0.4 mmol), was dissolved in 5 mL triflouroacetic acid (TFA) and added to the cooled solution. The mixture was stirred at 273 K for 2 h, concentrated *in vacuo*, taken up in 3 mL of water, and washed with 3x1 mL of diethyl ether. Hydrogen sulfide gas (H_2S) was bubbled into the aqueous solution for 15 min, the suspension was filtered through Celite and the filtrate was concentrated *in vacuo* to give 67 mg (yield 78%) of the di(trifluoroacetate) salt of the title compound as a pale green glass: ^{1}H NMR (600 MHz, H_2O:D_2O, 95:5, v/v) δ 3.51 (1H, dd, *J* 8, 16 Hz, βH), 3.67 (1H, dd, *J* 8, 16 Hz, βH), 4.51 (1H, dd, *J* 8 Hz, αH), 4.65 (3H, s, NCH_3), 8.75 (1H, s, Im^2H); ^{13}C NMR (600 MHz, H_2O:D_2O, 95:5, v/v) δ 26.4 (βC), 36.8 (NCH_3), 53.7 (αC), 122.0 (Im^5C), 133.8 (Im^4C), 139.0 (Im^2C), 172.7 (COOH); UV (λ_{max}, nm, H_2O) 237, 278 (shoulder) [67]; HRMS *m/z* [M+H][+] Calcd: 202.0650, Found: 202.0654.

(2*S*,2'*S*)-3,3'-[Disulfanediylbis(1-methyl-1*H*-imidazol-4,5-diyl)]bis(2-aminopropanoic acid), ovothiol disulfide (7). 50 mg (0.1 mmol) of compound (**6**) was taken up in 10 mL water, then air was bubbled through the solution for 1 h. NMR studies showed that the oxidation of (**6**) commenced quantitatively. Freeze-drying the solution yielded 49.4 mg (yield 99%) of the tetra(trifluoroacetate) salt of (**7**): ^{1}H NMR (600 MHz, H_2O:D_2O, 95:5, v/v) δ 2.35 (1H, dd, *J* 7.5, 16 Hz, βH), 2.53 (1H, dd, *J* 7.5, 16 Hz, βH), 3.38 (1H, dd, *J* 7.5 Hz, αH), 3.63 (3H, s, NCH_3), 7.72 (1H, s, Im^2H); $[\alpha]_D^{20}$

+74 (*c* 0.5, 0.1 mol/L HCl$_{(aq)}$) [67]; UV (λ_{max}, nm, 0.1 mol/L HCl$_{(aq)}$) 257; HRMS *m/z* [M+H]$^+$ Calcd: 400.0987, Found: 400.0988. Optical rotation was measured on a Jasco Model P-2000 polarimeter at the D line of sodium.

3.9.2 General procedures

Methyl ester formation was achieved by dissolving the reactant in 5 mL methanol and adding 1.5 equivalents of thionyl chloride at 273 K. The mixture was stirred at room temperature overnight, and then the solvent was evaporated *in vacuo* to give the title compound which was used in analytical experiments without purification. The synthesized products are itemized below.

Ovothiol disulfide dimethyl ester (8). ^{1}H NMR (600 MHz, H$_2$O:D$_2$O, 95:5, v/v) δ 2.72 (2H, dd, *J* 8, 20 Hz, βH), 2.88 (2H, dd, *J* 8, 20 Hz, βH), 3.61 (6H, s, OCH$_3$), 3.82 (2H, t, *J* 8 Hz, αH), 3.84 (6H, s, NCH$_3$), 8.01 (2H, s, Im^{2}H); HRMS *m/z* [M+H]$^+$ Calcd: 401.1066, Found: 401.1052.

Glutathione methyl ester (Gly) (9). ^{1}H NMR (600 MHz, H$_2$O:D$_2$O, 95:5, v/v) δ 1.91 (2H, m, βH(Glu)), 2.34 (2H, m, γH(Glu)), 2.75 (2H, m, βH(Cys)), 3.44 (1H, t, *J* 6 Hz, αH(Glu)), 3.61 (3H, s, OCH$_3$(Gly)), 3.89 (2H, dd, *J* 5, 18 Hz, αH(Gly)), 4.22 (1H, dd, *J* 2.5, 5 Hz, αH(Cys)); HRMS *m/z* [M+H]$^+$ Calcd: 322.1073, Found: 322.1012.

Glutathione dimethyl ester (10). ^{1}H NMR (600 MHz, H$_2$O:D$_2$O, 95:5, v/v) δ 2.21 (2H, m, βH(Glu)), 2.58 (2H, m, γH(Glu)), 2.94 (2H, m, βH(Cys)), 3.75 (3H, s, OCH$_3$(Gly)), 3.91 (3H, s, OCH$_3$(Glu)), 3.97 (1H, t, *J* 6 Hz, αH(Glu)), 4.04 (2H, d, *J* 6 Hz, αH(Gly)), 4.55 (1H, t, *J* 6 Hz, αH(Cys)); HRMS *m/z* [M+H]$^+$ Calcd: 336.1229, Found: 336.1574.

Cysteine methyl ester (11). ^{1}H NMR (600 MHz, H$_2$O:D$_2$O, 95:5, v/v) δ 3.94 (1H, t, *J* 5.5 Hz, αH), 3.79 (3H, s, OCH$_3$), 2.98 (1H, dd, *J* 6, 14 Hz, βH), 2.91 (1H, dd, *J* 5, 14 Hz, βH); HRMS *m/z* [M+H]$^+$ Calcd: 136.0432, Found: 136.0416.

Cystine dimethyl ester (12). ^{1}H NMR (600 MHz, H$_2$O:D$_2$O, 95:5, v/v) δ 4.40 (2H, dd, *J* 5, 7 Hz, αH), 3.85 (6H, s, OCH$_3$), 3.34 (2H, dd, *J* 5, 15 Hz, βH), 3.28 (2H, dd, *J* 7, 15 Hz, βH); HRMS *m/z* [M+H]$^+$ Calcd: 269.0630, Found: 269.0621.

Homocysteine methyl ester (13). ^{1}H NMR (600 MHz, $H_2O:D_2O$, 95:5, v/v) δ 4.25 (1H, t, *J* 8 Hz, αH), 3.84 (3H, s, OCH$_3$), 2.88 (2H, t, *J* 7 Hz, γH), 2.40 (2H, m, βH); HRMS *m/z* [M+H]$^+$ Calcd: 150.0589, Found: 150.0593.

Methionine methyl ester (14). ^{1}H NMR (600 MHz, $H_2O:D_2O$, 95:5, v/v) δ 4.30 (1H, t, *J* 6.5 Hz, αH), 3.85 (3H, s, OCH$_3$), 2.69 (2H, t, *J* 8 Hz, γH), 2.30 (2H, m, βH), 2.13 (3H, s, SCH$_3$); HRMS *m/z* [M+H]$^+$ Calcd: 164.0745, Found: 164.0751.

Homocystine dimethyl ester (15). ^{1}H NMR (600 MHz, $H_2O:D_2O$, 95:5, v/v) δ 4.31 (2H, t, *J* 7 Hz, αH), 3.86 (6H, s, OCH$_3$), 2.90 (4H, t, *J* 7 Hz, γH), 2.42 (4H, m, βH); HRMS *m/z* [M+H]$^+$ Calcd: 297.0943, Found 297.0957.

Penicillamine methyl ester (16). ^{1}H NMR (600 MHz, $H_2O:D_2O$, 95:5, v/v) δ 1.42 (3H, s, βCH$_3$), 1.45 (3H, s, βCH$_3$), 3.68 (1H, s, αH), 3.79 (3H, s, OCH$_3$); HRMS *m/z* [M+H]$^+$ Calcd: 164.0745, Found: 164.0724.

Penicillamine disulfide dimethyl ester (17). ^{1}H NMR (600 MHz, $H_2O:D_2O$, 95:5, v/v) δ 1.50 (3H, s, βCH$_3$), 1.57 (3H, s, βCH$_3$), 3.66 (3H, s, OCH$_3$), 4.19 (1H, s, αH); HRMS *m/z* [M+H]$^+$ Calcd: 325.1256, Found: 325.1296.

Amide formation was achieved by dissolving the reactant in 5 mL methanol and adding 0.5 mL concentrated ammonia. The mixture was stirred at room temperature overnight; subsequently the solvent was evaporated *in vacuo* to give the title compound which was used in analytical experiments without purification. The synthesized product is characterized below.

Ovothiol amide (18). ^{1}H NMR (600 MHz, $H_2O:D_2O$, 95:5, v/v) δ 3.26 (1H, dd, *J* 8, 15 Hz, βH), 3.29 (1H, dd, *J* 8, 15 Hz, βH), 3.76 (3H, s, NCH$_3$), 4.44 (1H, dd, *J* 7 Hz, αH), 8.26 (1H, s, Im^{2}H); HRMS *m/z* [M+H]$^+$ Calcd: 201.0810, Found: 201.0815.

S-methyl formation was achieved by dissolving the reactant in 5 mL of aqueous ammonia solution (pH=9) and adding 3 equivalents of CH$_3$I. The solution was stirred at room temperature for 1 h under N$_2$, and the excess ammonia was eliminated in vacuo.

The resulting aqueous solution was used in subsequent NMR experiments. The synthesized products are itemized below.

S-Methylovothiol (19). ^{1}H NMR (600 MHz, H_2O:D_2O, 95:5, v/v) δ 2.37 (3H, s, SCH_3), 3.19 (1H, dd, J 7, 15 Hz, βH), 3.25 (1H, dd, J 7, 15 Hz, βH), 3.78 (3H, s, NCH_3), 3.95 (1H, dd, J 8 Hz, αH), 8.72 (1H, s, Im[2]H); HRMS *m/z* [M+H][+] Calcd: 216.0961, Found: 216.0960.

S-Methylovothiol amide (20). ^{1}H NMR (600 MHz, H_2O:D_2O, 95:5, v/v) δ 3.26 (1H, dd, J 8, 15 Hz, βH), 3.28 (1H, dd, J 8, 15 Hz, βH), 3.82 (3H, s, NCH_3), 4.25 (1H, dd, J 7 Hz, αH), 8.74 (1H, s, Im[2]H); UV (λ_{max}, nm, H_2O) 198, 225 (shoulder); HRMS *m/z* [M+H][+] Calcd: 215.0967, Found: 215.0959.

S-Methylcysteamine (21). ^{1}H NMR (600 MHz, H_2O:D_2O, 95:5, v/v) δ 3.24 (2H, t, J 7 Hz, αH), 2.82 (2H, t, J 7 Hz, βH), 2.73 (3H, s, SCH_3); HRMS *m/z* [M+H][+] Calcd: 92.0534, Found: 92.0567.

S-Methylcysteine (22). ^{1}H NMR (600 MHz, H_2O:D_2O, 95:5, v/v) δ 3.94 (1H, dd, J 5, 8 Hz, αH), 3.09 (1H, dd, J 5, 15 Hz, βH), 2.99 (1H, dd, J 8, 15 Hz, βH), 2.15 (3H, s, SCH3); HRMS *m/z* [M+H][+] Calcd: 136.0432, Found: 136.0420.

S-Methylcysteine methyl ester (23). ^{1}H NMR (600 MHz, H_2O:D_2O, 95:5, v/v) δ 4.22 (1H, dd, J 5, 7.5 Hz, αH), 3.83 (3H, s, OCH_3), 3.11 (1H, dd, J 5, 15 Hz, βH), 3.00 (1H, dd, J 7.5, 15 Hz, βH), 2.14 (3H, s, SCH_3); HRMS *m/z* [M+H][+] Calcd: 150.0589, Found: 150.0583.

S-Methylpenicillamine (24). ^{1}H NMR (600 MHz, H_2O:D_2O, 95:5, v/v) δ 1.31 (3H, s, βCH_3), 1.52 (3H, s, βCH_3), 2.07 (3H, s, SCH_3), 3.67 (1H, s, αH); HRMS *m/z* [M+H][+] Calcd: 164.0745, Found: 164.0687.

S-Methylpenicillamine methyl ester (25). ^{1}H NMR (600 MHz, H_2O:D_2O, 95:5, v/v) δ 1.48 (3H, s, βCH_3), 1.56 (3H, s, βCH_3), 1.92 (3H, s, SCH_3), 3.71 (3H, s, OCH_3), 3.88 (1H, s, αH); HRMS *m/z* [M+H][+] Calcd: 178.0902, Found: 178.0930.

When necessary the thiol formation from a disulfide was achieved with reduction. The reactant was dissolved in 5 ml of methanol and 2.5 equivalents of sodium tetrahydroborate were added. After stirring at ambient temperature for 1 h, the reaction mixture was evaporated *in vacuo* to yield the title compound which was used in analytical experiments without purification. The synthesized product is characterized below.

Homocysteine (26). ^{1}H NMR (600 MHz, H_2O:D_2O, 95:5, v/v) δ 3.85 (1H, t, *J* 7 Hz, αH), 2.83 (2H, t, *J* 8 Hz, γH), 2.27 (2H, m, βH); HRMS *m/z* [M+H]$^+$ Calcd: 136.0432, Found: 136.0442.

Dihydrolipoic acid (27). ^{1}H NMR (600 MHz, H_2O:D_2O, 95:5, v/v) δ 1.40 (1H, m, C^4H_2), 1.46 (1H, m, C^4H_2), 1.54 (1H, m, C^5H_2), 1.54 (2H, m, C^3H_2), 1.69 (1H, m, C^5H_2), 1.78 (1H, m, C^7H_2), 1.94 (1H, m, C^7H_2), 2.18 (2H, t, *J* 7.5 Hz, C^2H_2), 2.67 (1H, m, C^8H_2), 2.72 (1H, m, C^8H_2), 3.02 (1H, m, C^6H); HRMS *m/z* [M+H]$^+$ Calcd: 209.0670, Found: 209.0655.

Dihydrolipoamide (28). ^{1}H NMR (600 MHz, H_2O:D_2O, 95:5, v/v) δ 1.44 (1H, m, C^4H_2), 1.51 (1H, m, C^4H_2), 1.60 (1H, m, C^5H_2), 1.60 (2H, m, C^3H_2), 1.68 (1H, m, C^5H_2), 1.78 (1H, m, C^7H_2), 1.93 (1H, m, C^7H_2), 2.28 (2H, t, *J* 7.7 Hz, C^2H_2), 2.67 (1H, m, C^8H_2), 2.71 (1H, m, C^8H_2), 3.01 (1H, m, C^6H), 6.22 (1H, s, NH), 7.54 (1H, s, NH); HRMS *m/z* [M+H]$^+$ Calcd: 208.0830, Found: 208.0838.

When necessary the homodisulfide formation from a thiol was achieved with *in situ* oxidation. The thiol was dissolved in 2% aqueous hydrogen peroxide solution and the pH adjusted to 8.5. The solution was stirred for 30 minutes, and the resulting aqueous solution was used in subsequent NMR experiments. The synthesized products are itemized below.

Glutathione disulfide tetramethyl ester (29) ^{1}H NMR (600 MHz, H_2O:D_2O, 95:5, v/v) δ 2.05 (4H, m, γH(Glu)), 2.18 (4H, m, βH(Glu)), 3.05 (4H, m, βH(Cys)), 3.68 (6H, s, OCH$_3$(Gly)), 3.87 (6H, s, OCH$_3$(Glu)), 3.45 (2H, t, *J* 6 Hz, αH(Glu)), 4.16 (4H, d, *J* 6

Hz, αH(Gly)), 4.81 (2H, t, J 6 Hz, αH(Cys)); HRMS m/z [M+H]$^+$ Calcd: 669.2224, Found: 669.2222.

Glutathione disulfide dimethyl ester (Gly) (30) ^{1}H NMR (600 MHz, H_2O:D_2O, 95:5, v/v) δ 2.04 (4H, m, βH(Glu)), 2.11 (4H, m, γH(Glu)), 3.11 (4H, m, βH(Cys)), 3.49 (2H, t, J 6 Hz, αH(Glu)), 3.68 (6H, s, OCH$_3$(Gly)), 4.16 (4H, dd, J 5, 18 Hz, αH(Gly)), 4.81 (2H, dd, J 2.5, 5 Hz, αH(Cys)); HRMS m/z [M+H]$^+$ Calcd: 641.1911, Found: 641.1912.

Cystamine (31). ^{1}H NMR (600 MHz, H_2O:D_2O, 95:5, v/v) δ 3.40 (4H, t, J 7 Hz, αH), 3.02 (4H, t, J 7 Hz, βH); HRMS m/z [M+H]$^+$ Calcd: 153.0520, Found: 153.0517.

Cystine (32). ^{1}H NMR (600 MHz, H_2O:D_2O, 95:5, v/v) δ 4.23 (2H, dd, J 4, 9 Hz, αH), 3.41 (2H, dd, J 4, 15 Hz, βH), 3.22 (2H, dd, J 9, 15 Hz, βH); HRMS m/z [M+H]$^+$ Calcd: 241.0317, Found: 241.0320.

Penicillamine disulfide (33). ^{1}H NMR (600 MHz, H_2O:D_2O, 95:5, v/v) δ 1.44 (3H, s, βCH$_3$), 1.55 (3H, s, βCH$_3$), 4.01 (1H, s, αH); HRMS m/z [M+H]$^+$ Calcd: 297.0943, Found: 297.1017.

4. RESULTS

The determination of species-specific protonation constants for every compound was performed based on case-tailored deduction methods, which nonetheless share a common underlying approach. The design of the deductive method is epitomized in detail for the simple case of cysteamine. The noteworthy alterations in the deductive method of the remaining compounds will be highlighted however, due to the intrinsic complexity of microspeciation of molecular entities with higher number of basic sites: microspecies are coexisting, inseparable solution entities, with different location and/or number of protons at the basic sites on a definite covalent skeleton of the molecule, therefore their concentrations can only be measured indirectly [33]. Since the number of microspecies increases exponentially with the number of basic sites, complete, correct microspeciation for non-symmetrical, compact molecules has so far been reported for molecules of up to three basic sites. Ovothiol, for instance, has four distinct basic sites with an omni-interactive molecular structure, in which the protonation of any sites has an effect of *a priori* unknown magnitude on the basicity of every other site. Studies have shown [64] that complete microspeciation for molecules of four or more basic sites cannot be carried out without importing additional information, even though the protonation percentage is known for every site at each pH.

4.1 The microscopic protonation constants of cysteamine

Cysteamine was titrated under near physiological conditions and non-linear regression analysis of the ^{1}H NMR chemical shift-pH profiles afforded the macroscopic protonation constants presented in Table 1. The relationships between the macroscopic and microscopic protonation constants (equivalent to equations (9) and (11)) actualized for cysteamine are:

$$K_1 = k^N + k^S \tag{17}$$

$$\beta_2 = k^{\mathrm{N}} k_{\mathrm{N}}^{\mathrm{S}} = k^{\mathrm{S}} k_{\mathrm{S}}^{\mathrm{N}} \tag{18}$$

Thus, besides the macroconstants, the complete microspeciation of cysteamine needs at least one additional datum. This can be obtained via a deductive method, wherein the possible closest model of a minor microspecies is introduced and some appropriate protonation constant(s) of the model compound(s) is/are regarded as constituent protonation constants of the parent molecule. In the case of cysteamine, *S*-methylcysteamine was used to model the microspecies, in which the thiolate moiety is protonated. Therefore, the macroscopic protonation constant of *S*-methylcysteamine (Table 1) was equated to $k_{\mathrm{S}}^{\mathrm{N}}$ of cysteamine. The remaining microscopic protonation constants were calculated using equations (17) and (18), and are presented in Table 1. These data also yielded the interactivity parameter between the amino and thiolate groups:

$$\log \Delta E_{\mathrm{N/S}} = \log k^{\mathrm{N}} - \log k_{\mathrm{S}}^{\mathrm{N}} = \log k^{\mathrm{S}} - \log k_{\mathrm{N}}^{\mathrm{S}} \tag{19}$$

The interactivity parameter shows to what extent the protonation of site A reduces the basicity of site B, and vice versa. The interactivity parameter is generally considered to be the most invariant quantity in analogous moieties of different compounds and also in various protonation states of the neighboring moiety in the same molecule [60].

Table 1. The macroscopic and microscopic protonation constants (298 K, 0.15 mol/L ionic strength), and interactivity parameters of cysteamine, cystamine and their model compound in log units ±s.d.

Cysteamine		Cystamine	
Macroscopic Protonation Constants			
Cysteamine		Cystamine	
$\log K_1$	10.88±0.01	$\log K_1$	9.61±0.02
$\log K_2$	8.34±0.01	$\log K_2$	8.76±0.02
S-Methylcysteamine			
$\log K$	9.55±0.01		
Microscopic Protonation Constants			
$\log k^N$	10.85±0.01	$\log k^N$	9.31±0.02
$\log k^S$	9.67±0.01	$\log k_N^{N'}$	9.06±0.02
$\log k_N^S$	8.37±0.01		
$\log k_S^N$	9.55±0.01		
Interactivity Parameters			
$\log\Delta E_{N/S}$	1.30±0.01	$\log\Delta E_{N/N'}$	0.25±0.03

4.2 The microscopic protonation constants of cystamine

Cystamine, being the disulfide of cysteamine, is a symmetric molecule with two basic nitrogens, which can be arbitrarily named N and N'. Due to symmetry, their basicities are identical:

$$k^N = k^{N'} \tag{20}$$

$$k_{N'}^N = k_N^{N'} \tag{21}$$

This reduces the multivariable problem to a system with two unknowns only, which can be resolved using relationships derived from equations (9) and (11):

$$\log k^{\mathrm{N}} = \log K_1 - \log 2 \qquad (22)$$

$$\log k_{\mathrm{N}}^{\mathrm{N'}} = \log K_2 + \log 2 \qquad (23)$$

Macroscopic protonation constants from ^{1}H NMR-pH titration data and calculated microscopic protonation constants, along with the interactivity parameter between the two amino groups ($\log\Delta E_{\mathrm{N/N'}}$) are presented in Table 1.

4.3 The microscopic protonation constants of cysteine, homocysteine, and penicillamine

Cysteine, homocysteine, and penicillamine were titrated under near physiological conditions to afford the macroscopic protonation constants (Table 2, 3, 4). The microspeciation scheme of a tridendate molecule is a multivariable problem with 7 unknowns. Therefore, in addition to the three macroscopic protonation constants, four further quantities have to be introduced to elucidate all the microconstants. The kind and number of extra pieces of information to be introduced depend on the acid-base properties of the sites in the parent compounds. Chemical evidences clearly indicate that the inherent basicity decreases in the amino, thiolate, carboxylate order, in which the basicity of thiolate is "comparably lower", whereas the basicity of the carboxylate is typically "orders of magnitude lower" than that of the amino group. Consequently, those microspecies in which the carboxylate site is protonated, but the amino is not, are "orders of magnitude minor" (omm) ones, while those in which the thiolate is protonated, but the amino is not, are expected to be "relative minor" (rm) ones. Omm microspecies influence the analytical signals (NMR, UV, etc.) insignificantly, but they may be the reactive species in highly specific biochemical processes [57]. A complete microspeciation inevitably needs auxiliary derivative compounds that mimic the omm microspecies, and in many cases the rm microspecies too. The possible closest mimicry compounds of the d, c, and g cysteine microspecies are cysteine methyl ester, *S*-methylcysteine, and *S*-methylcysteine methyl ester, respectively, where the methyl moiety at the carboxylate or thiolate site keeps the site in question in its neutral form,

and has electronic effect on the rest of the molecule highly similar to the –COOH and –SH moiety, respectively [58]. The macroscopic protonation constants of the model compounds were also attained using NMR-pH titrations. As a subsequent step, the microscopic protonation constants were calculated using the principles in equations (9) and (11), bearing in mind that the macroscopic protonation constants of the model compounds are regarded as constituents of the cysteine (and homocysteine, penicillamine) microspeciation scheme.

4.4 The microscopic protonation constants of cystine, homocystine, and penicillamine disulfide

The microspeciation of cystine, homocystine, and penicillamine disulfide is inherently simplified by the symmetry of the molecular structure, and also the well-separated protonation pH range of the two amino and two carboxyl groups. The opposite amino and carboxylate groups are regarded chemically identical. This results in certain equalities among the microscopic protonation constants: $k^N = k^{N'}$, $k^O = k^{O'}$, etc. Furthermore, because of the large gap between the first and last two protonation steps, these steps can be regarded as practically independent systems. The change in ^{1}H NMR chemical shift recorded during the first two protonation steps is essentially generated by the protonation of the two amino groups, since the mono- and biprotonated ligands where any of the two carboxylate groups is protonated are orders of magnitude minor. The microscopic protonation constants of the major pathways of the microspeciation can therefore be calculated using equations (24)-(27).

$$\log k^N = \log K_1 - \log 2 \tag{24}$$

$$\log k_N^{N'} = \log K_2 + \log 2 \tag{25}$$

$$\log k_{NN'}^O = \log K_3 - \log 2 \tag{26}$$

$$\log k_{ONN'}^{O'} = \log K_4 + \log 2 \tag{27}$$

In order to characterize the orders of magnitude minor processes too, the dimethyl ester derivatives were applied to model the microspecies where both carboxylate groups are protonated. Using the principles as above, the remaining microscopic protonation constants were attained. All macroscopic and microscopic protonation constants along with the interactivity parameters are compiled in Table 2, 3, and 4.

Table 2. The macroscopic and microscopic protonation constants (298 K, 0.15 mol/L ionic strength), and interactivity parameters of cysteine, cystine and their model compounds in log units ±s.d.

Cysteine and its derivatives				Cystine and its derivative			
Macroscopic Protonation Constants							
Cysteine		Cysteine methyl ester		Cystine		Cystine dimethyl ester	
$\log K_1$	10.39±0.02	$\log K_1$	9.03±0.01	$\log K_1$	9.17±0.01	$\log K_1$	6.80±0.02
$\log K_2$	8.52±0.02	$\log K_2$	6.87±0.01	$\log K_2$	8.19±0.01	$\log K_2$	5.86±0.03
$\log K_3$	2.02±0.01	*S*-Methylcysteine		$\log K_3$	2.25±0.03		
S-Methylcysteine methyl ester		$\log K_1$	8.84±0.01	$\log K_4$	1.49±0.04		
$\log K$	6.95±0.01	$\log K_2$	2.02±0.01				
Microscopic Protonation Constants							
$\log k^{N}$	10.15±0.02	$\log k_S^{O}$	3.91±0.02	$\log k^{N}$	8.87±0.01	$\log k_{NN'}^{O}$	1.95±0.03
$\log k^{S}$	10.07±0.03	$\log k_O^{N}$	8.26±0.01	$\log k^{O}$	4.30±0.04	$\log k_{O'N}^{N'}$	6.60±0.01
$\log k^{O}$	5.03±0.03	$\log k_O^{S}$	8.95±0.01	$\log k_N^{N'}$	8.49±0.01	$\log k_{O'N}^{O}$	2.25±0.07
$\log k_N^{S}$	8.76±0.04	$\log k_{SN}^{O}$	2.02±0.02	$\log k_N^{O'}$	3.84±0.03	$\log k_{ON}^{N'}$	8.05±0.03
$\log k_N^{O}$	3.14±0.04	$\log k_{ON}^{S}$	7.64±0.01	$\log k_N^{O}$	2.41±0.04	$\log k_{ON}^{O'}$	3.68±0.04
$\log k_S^{N}$	8.84±0.01	$\log k_{OS}^{N}$	6.95±0.01	$\log k_O^{N'}$	8.39±0.02	$\log k_{OO'}^{N}$	6.50±0.02
				$\log k_O^{N}$	6.98±0.04	$\log k_{ONN'}^{O'}$	1.79±0.04
				$\log k_O^{O'}$	4.14±0.06	$\log k_{OO'N}^{N'}$	6.16±0.03
Interactivity Parameters							
$\log\Delta E_{N/S}$	1.31±0.01	$\log\Delta E_{S/O}$	1.12±0.03	$\log\Delta E_{N/O}$	1.89±0.01	$\log\Delta E_{N/N'}$	0.38±0.01
$\log\Delta E_{N/O}$	1.89±0.01			$\log\Delta E_{N/O'}$	0.48±0.02	$\log\Delta E_{O/O'}$	0.16±0.05

Table 3. The macroscopic and microscopic protonation constants (298 K, 0.15 mol/L ionic strength), and interactivity parameters of homocysteine, homocystine and their model compounds in log units ±s.d.

41

Homocysteine and its derivatives				Homocystine and its derivative			
Macroscopic Protonation Constants							
Homocysteine		Homocysteine methyl ester		Homocystine		Homocystine dimethyl ester	
$\log K_1$	10.35±0.02	$\log K_1$	9.38±0.04	$\log K_1$	9.64±0.03	$\log K_1$	7.32±0.02
$\log K_2$	8.65±0.02	$\log K_2$	7.22±0.01	$\log K_2$	8.75±0.03	$\log K_2$	6.42±0.01
$\log K_3$	2.21±0.02	Methionine		$\log K_3$	2.35±0.04		
Methionine methyl ester		$\log K_1$	9.15±0.01	$\log K_4$	1.64±0.04		
$\log K$	7.25±0.01	$\log K_2$	2.12±0.01				
Microscopic Protonation Constants							
$\log k^{N}$	10.10±0.02	$\log k_S^{O}$	4.02±0.02	$\log k^{N}$	9.34±0.03	$\log k_{NN'}^{O}$	2.05±0.04
$\log k^{S}$	9.94±0.04	$\log k_O^{N}$	8.20±0.01	$\log k^{O}$	4.37±0.05	$\log k_{O'N}^{N'}$	7.15±0.03
$\log k^{O}$	4.61±0.04	$\log k_O^{S}$	9.35±0.01	$\log k_N^{N'}$	9.05±0.03	$\log k_{O'N}^{O}$	2.37±0.07
$\log k_N^{S}$	8.99±0.04	$\log k_{SN}^{O}$	2.12±0.02	$\log k_N^{O'}$	3.95±0.04	$\log k_{ON}^{N'}$	8.62±0.01
$\log k_N^{O}$	2.71±0.04	$\log k_{ON}^{S}$	8.40±0.01	$\log k_N^{O}$	2.47±0.05	$\log k_{ON}^{O'}$	3.84±0.04
$\log k_S^{N}$	9.15±0.01	$\log k_{OS}^{N}$	7.25±0.01	$\log k_O^{N'}$	8.92±0.02	$\log k_{OO'}^{N}$	7.02±0.02
				$\log k_O^{N}$	7.44±0.05	$\log k_{ONN'}^{O'}$	1.94±0.04
				$\log k_O^{O'}$	4.27±0.07	$\log k_{OO'N}^{N'}$	6.72±0.01
Interactivity Parameters							
$\log \Delta E_{N/S}$	0.95±0.01	$\log \Delta E_{S/O}$	0.59±0.03	$\log \Delta E_{N/O}$	1.90±0.01	$\log \Delta E_{N/N'}$	0.29±0.04
$\log \Delta E_{N/O}$	1.90±0.01			$\log \Delta E_{N/O'}$	0.42±0.04	$\log \Delta E_{O/O'}$	0.11±0.06

Table 4. The macroscopic and microscopic protonation constants (298 K, 0.15 mol/L ionic strength), and interactivity parameters of penicillamine, penicillamine disulfide and their model compounds in log units ±s.d.

Penicillamine and its derivatives				Penicillamine disulfide and its derivative			
Macroscopic Protonation Constants							
Penicillamine		Penicillamine methyl ester		Penicillamine disulfide		Penicillamine disulfide dimethyl ester	
$\log K_1$	10.80±0.01	$\log K_1$	8.99±0.01	$\log K_1$	9.48±0.01	$\log K_1$	7.23±0.02
$\log K_2$	8.07±0.01	$\log K_2$	6.90±0.01	$\log K_2$	8.57±0.03	$\log K_2$	6.32±0.01
$\log K_3$	2.04±0.01	*S*-Methylpenicillamine		$\log K_3$	2.34±0.02		
S-Methylpenicillamine methyl ester		$\log K_1$	9.53±0.01	$\log K_4$	1.61±0.04		
$\log K$	7.65±0.01	$\log K_2$	2.04±0.01				
Microscopic Protonation Constants							
$\log k^{\mathrm{N}}$	10.78±0.01	$\log k_{\mathrm{S}}^{\mathrm{O}}$	3.92±0.01	$\log k^{\mathrm{N}}$	9.18±0.03	$\log k_{\mathrm{NN'}}^{\mathrm{O}}$	2.04±0.03
$\log k^{\mathrm{S}}$	9.34±0.01	$\log k_{\mathrm{O}}^{\mathrm{N}}$	8.90±0.01	$\log k^{\mathrm{O}}$	4.29±0.02	$\log k_{\mathrm{O'N}}^{\mathrm{N'}}$	6.99±0.03
$\log k^{\mathrm{O}}$	5.02±0.01	$\log k_{\mathrm{O}}^{\mathrm{S}}$	8.24±0.01	$\log k_{\mathrm{N}}^{\mathrm{N'}}$	8.87±0.03	$\log k_{\mathrm{O'N}}^{\mathrm{O}}$	2.28±0.06
$\log k_{\mathrm{N}}^{\mathrm{S}}$	8.09±0.01	$\log k_{\mathrm{SN}}^{\mathrm{O}}$	2.04±0.01	$\log k_{\mathrm{N}}^{\mathrm{O'}}$	3.92±0.02	$\log k_{\mathrm{ON}}^{\mathrm{N'}}$	8.50±0.01
$\log k_{\mathrm{N}}^{\mathrm{O}}$	3.14±0.01	$\log k_{\mathrm{ON}}^{\mathrm{S}}$	6.99±0.01	$\log k_{\mathrm{N}}^{\mathrm{O}}$	2.41±0.01	$\log k_{\mathrm{ON}}^{\mathrm{O'}}$	3.79±0.05
$\log k_{\mathrm{S}}^{\mathrm{N}}$	9.53±0.01	$\log k_{\mathrm{OS}}^{\mathrm{N}}$	7.65±0.01	$\log k_{\mathrm{O}}^{\mathrm{N'}}$	8.81±0.02	$\log k_{\mathrm{OO'}}^{\mathrm{N}}$	6.93±0.02
				$\log k_{\mathrm{O}}^{\mathrm{N}}$	7.30±0.06	$\log k_{\mathrm{ONN'}}^{\mathrm{O'}}$	1.91±0.04
				$\log k_{\mathrm{O}}^{\mathrm{O'}}$	4.16±0.06	$\log k_{\mathrm{OO'N}}^{\mathrm{N'}}$	6.62±0.02
Interactivity Parameters							
$\log\Delta E_{\mathrm{N/S}}$	1.25±0.01	$\log\Delta E_{\mathrm{S/O}}$	1.10±0.01	$\log\Delta E_{\mathrm{N/O}}$	1.88±0.01	$\log\Delta E_{\mathrm{N/N'}}$	0.29±0.03
$\log\Delta E_{\mathrm{N/O}}$	1.88±0.01			$\log\Delta E_{\mathrm{N/O'}}$	0.37±0.04	$\log\Delta E_{\mathrm{O/O'}}$	0.11±0.05

4.5 The microscopic protonation constants of glutathione

In glutathione the glutamyl, glycinyl, and cysteinyl α protons were monitored throughout the pH range with high resolution ^{1}H NMR. Due to inherent basicities of the four basic centers in GSH, at basic pH predominantly the amino and thiolate moieties protonate in an overlapping manner. Upon lowering the pH, the separate, yet again simultaneous protonation of the two carboxylates takes place. These protonation pathways comprise the major pathway of the GSH microspeciation scheme. Furthermore, it is apparent from the chemical shift-pH profiles that each α hydrogen is selectively (or at least overwhelmingly rendering other protonations insignificant) perturbed only by the basic moiety in its immediate proximity; i.e. the glycinyl α hydrogen is selective for the glycinyl carboxylate, the cysteinyl α hydrogen is selective for the thiolate, and the glutamyl α hydrogen is selective for the adjacent amino and glutamyl carboxylate protonations. Therefore by fitting sigmoid curves that specifically express the protonation fraction of each site, one can attain the microscopic protonation constants of the major pathway. For the pH range 6-14 the following function was fitted to the data of the glutamyl and cysteinyl α hydrogens:

$$\delta_{\text{obs}}(\text{pH}) = \frac{(\delta_{\text{HL}} - \delta_{\text{L}})(k^{\text{X}}[\text{H}^+] + K_1 K_2[\text{H}^+]^2)}{1 + (k^{\text{N}} + k^{\text{S}})[\text{H}^+] + K_1 K_2[\text{H}^+]^2} + \delta_{\text{L}} \tag{28}$$

where $\delta_{\text{obs(pH)}}$ is the observed chemical shift of the given nucleus at a particular pH, δ_{HL} and δ_{L} are the limiting chemical shifts of the protonated and deprotonated states, and k^{N} or k^{S} was used in lieu of k^{X} for the data of glutamyl and cysteinyl α hydrogens, respectively. The next separate protonation region is that of the two carboxylates; for the pH range 0-6 the following function was fitted to the data of the glutamyl and glycinyl α hydrogens:

$$\delta_{\text{obs}}(\text{pH}) = \frac{(\delta_{\text{HL}} - \delta_{\text{L}})(k_{\text{NS}}^{\text{X}}[\text{H}^+] + K_3 K_4[\text{H}^+]^2)}{1 + (k_{\text{NS}}^{\text{G}} k_{\text{NS}}^{\text{E}})[\text{H}^+] + K_3 K_4[\text{H}^+]^2} + \delta_{\text{L}} \tag{29}$$

where $\delta_{\mathrm{obs(pH)}}$ is the observed chemical shift of the given nucleus at a particular pH, δ_{HL} and δ_{L} are the limiting chemical shifts of the protonated and deprotonated states, and $k_{\mathrm{NS}}{}^{\mathrm{G}}$ or $k_{\mathrm{NS}}{}^{\mathrm{E}}$ was used in lieu of $k_{\mathrm{NS}}{}^{\mathrm{X}}$ for the data of glycinyl and glutamyl α hydrogens, respectively. After attaining the macroconstants and k^{N}, k^{S}, $k_{\mathrm{NS}}{}^{\mathrm{G}}$, $k_{\mathrm{NS}}{}^{\mathrm{E}}$ values, the remaining constants of the major pathway could be calculated with equations analogous to equations (9) and (11), by regarding the two separate protonation regions as two bidentate protonation processes; i.e. assuming $k_{\mathrm{NS}}{}^{\mathrm{G}}+k_{\mathrm{NS}}{}^{\mathrm{E}}=K_3$. These data also afford the amino-thiolate interactivity parameter ($\log\Delta E_{\mathrm{N/S}}$) and the interactivity parameter between the two carboxylates ($\log\Delta E_{\mathrm{G/E}}$).

With the knowledge of the microscopic constants of the major pathway the rest of the microspeciation scheme can be elucidated with the help of two model compounds. Glutathione dimethyl ester (G(OMe)$_2$SH) and glutathione methyl ester (methylated at Gly, abbreviated as GOMe$_{\mathrm{Gly}}$SH) mimic the k and d microspecies. By using the evaluation method described above macroscopic and microscopic protonation constants of the model compounds were determined. All of the macroconstants of the model compounds are also compiled in Table 5; it can be seen that the $k_{\mathrm{NSG}}{}^{\mathrm{E}}$ value determined with two independent methods is in excellent agreement (compare $k_{\mathrm{NSG}}{}^{\mathrm{E}}$ with K_3 of GOMe$_{\mathrm{Gly}}$SH). The remaining microconstants were calculated with the interactivity parameters afforded by the model compounds. All species-specific protonation constants of GSH with the 6 interactivity parameters are compiled in Table 5.

Table 5. The macroscopic and microscopic protonation constants (298 K, 0.15 mol/L ionic strength), and interactivity parameters of glutathione and related model compounds in log units ± s.d. The microscopic protonation constants of the major pathway are in bold.

		GSH		$GOMe_{Gly}SH$		$G(OMe)_2SH$
	$\log K_1$	9.65 ±0.01	$\log K_1$	9.44 ±0.04	$\log K_1$	8.64 ±0.01
	$\log K_2$	8.78 ±0.01	$\log K_2$	8.46 ±0.03	$\log K_2$	7.06 ±0.01
	$\log K_3$	3.52 ±0.01	$\log K_3$	2.23 ±0.01		
	$\log K_4$	2.22 ±0.01				
Microscopic protonation constants						
amino		thiolate		carboxylate (Gly)		carboxylate (Glu)
$\mathbf{\log k^N}$ **9.49 ±0.01**		$\mathbf{\log k^S}$ **9.26 ±0.01**		$\log k^G$ 4.04 ±0.04		$\log k^E$ 4.53 ±0.03
$\mathbf{\log k_S^N}$ **9.17 ±0.02**		$\mathbf{\log k_N^S}$ **8.94 ±0.02**		$\log k_N^G$ 3.89 ±0.02		$\log k_N^E$ 2.60 ±0.03
$\log k_G^N$ 9.31 ±0.01		$\log k_G^S$ 8.87 ±0.02		$\log k_S^G$ 3.65 ±0.03		$\log k_S^E$ 4.28 ±0.02
$\log k_E^N$ 7.56 ±0.01		$\log k_E^S$ 9.01 ±0.02		$\log k_E^G$ 3.94 ±0.04		$\log k_G^E$ 4.43 ±0.03
$\log k_{SG}^N$ 9.01 ±0.02		$\log k_{NG}^S$ 8.59 ±0.05		$\mathbf{\log k_{NS}^G}$ **3.50 ±0.01**		$\mathbf{\log k_{NS}^E}$ **2.35 ±0.02**
$\log k_{SE}^N$ 7.24 ±0.02		$\log k_{NE}^S$ 8.71 ±0.03		$\log k_{NE}^G$ 3.79 ±0.03		$\log k_{NG}^E$ 2.50 ±0.02
$\log k_{GE}^N$ 7.38 ±0.01		$\log k_{GE}^S$ 8.62 ±0.01		$\log k_{SE}^G$ 3.55 ±0.03		$\log k_{SG}^E$ 4.18 ±0.01
$\log k_{SGE}^N$ 7.08 ±0.02		$\log k_{NGE}^S$ 8.32 ±0.02		$\mathbf{\log k_{NSE}^G}$ **3.40 ±0.02**		$\mathbf{\log k_{NSG}^E}$ **2.25 ±0.01**
Interactivity parameters						
$\log\Delta E_{N/E}$ 1.93 ±0.01		$\log\Delta E_{N/S}$ 0.32 ±0.02		$\log\Delta E_{N/G}$ 0.18 ±0.02		
$\log\Delta E_{S/G}$ 0.39 ±0.02		$\log\Delta E_{S/E}$ 0.25 ±0.02		$\log\Delta E_{G/E}$ 0.10 ±0.02		

4.6 The microscopic protonation constants of glutathione disulfide

Since the microspeciation of the major pathway of GSSG has already been thoroughly elucidated under the same conditions as presented here [26] (macroscopic protonation constants of GSSG: $\log K_1$=9.71 ±0.01, $\log K_2$=8.95 ±0.02, $\log K_3$=3.91 ±0.02, $\log K_4$=3.23 ±0.03, $\log K_5$=2.41 ±0.03, $\log K_6$=1.79 ±0.05), only the minor pathway needed investigation. GSSG diethyl ester (at the glycine residues) was also investigated by [26] and the carboxylate constants showed excellent agreement with the native GSSG data, therefore GSSG dimethyl ester was only titrated above pH 7. The microscopic protonation constants of the symmetric model compounds (GSSG dimethyl ester (Gly) and GSSG tetramethyl ester) were related to microspeciation scheme of the GSSG. Furthermore, these data afforded the interactivity parameters pertaining to the minor pathways. Because of symmetry, the microscopic protonation constants of the disulfide model compounds could be readily calculated. Introducing the one-side interactivity parameters of GSH as constituents of the GSSG system, all of the remaining GSSG microconstants could be calculated using the interactivity parameters applied to GSSG. The microscopic protonation constants and interactivity parameters of GSSG are compiled in Table 6.

Table 6. The microscopic protonation constants (298 K, 0.15 mol/L ionic strength), and interactivity parameters of glutathione disulfide in log units ± s.d. The microscopic protonation constants of the major pathway are in bold, taken from [26]. *the one-side interactivity parameters introduced from the microspeciation of GSH.

Microscopic protonation constants					
amino		carboxylate (Gly)		carboxylate (Glu)	
$\log k^{N}$	**9.41 ±0.01**	$\log k^{G}$	3.92 ±0.03	$\log k^{E}$	4.45 ±0.03
$\log k_N^{N'}$	**9.25 ±0.02**	$\log k_N^{G'}$	3.77 ±0.02	$\log k_N^{E''}$	4.35 ±0.02
$\log k_G^{N'}$	9.26 ±0.02	$\log k_N^{G}$	3.74 ±0.03	$\log k_N^{E}$	2.52 ±0.03
$\log k_G^{N}$	9.23 ±0.02	$\log k_G^{G'}$	3.78 ±0.03	$\log k_G^{E''}$	4.34 ±0.03
$\log k_E^{N'}$	9.31 ±0.02	$\log k_E^{G'}$	3.81 ±0.03	$\log k_G^{E}$	4.34 ±0.03
$\log k_E^{N}$	7.48 ±0.01	$\log k_E^{G}$	3.81 ±0.03	$\log k_E^{E'}$	4.37 ±0.04
$\log k_{NG'}^{N'}$	9.07 ±0.03	**$\log k_{NN'}^{G}$**	**3.59 ±0.01**	**$\log k_{NN'}^{E}$**	**2.42 ±0.02**
$\log k_{NG}^{N'}$	9.09 ±0.02	$\log k_{NG}^{G}$	3.60 ±0.02	$\log k_{NG'}^{E'}$	4.24 ±0.02
$\log k_{NE'}^{N'}$	7.32 ±0.02	$\log k_{NG}^{G'}$	3.63 ±0.02	$\log k_{NG}^{E}$	2.41 ±0.03
$\log k_{NE}^{N'}$	9.17 ±0.03	$\log k_{NE'}^{G}$	3.63 ±0.02	$\log k_{NG}^{E'}$	4.24 ±0.02
$\log k_{GG'}^{N}$	9.08 ±0.01	$\log k_{NE'}^{G'}$	3.66 ±0.02	$\log k_{NG}^{E}$	2.41 ±0.03
$\log k_{GE'}^{N}$	9.13 ±0.03	$\log k_{NE}^{G'}$	3.66 ±0.02	$\log k_{NE}^{E}$	2.44 ±0.03
$\log k_{GE'}^{N'}$	7.33 ±0.02	$\log k_{NE}^{G}$	3.63 ±0.02	$\log k_{NE}^{E'}$	4.27 ±0.02
$\log k_{GE}^{N'}$	9.16 ±0.02	$\log k_{GE'}^{G'}$	3.67 ±0.03	$\log k_{GG'}^{E}$	4.23 ±0.05
$\log k_{GE}^{N}$	7.30 ±0.02	$\log k_{GE}^{G'}$	3.67 ±0.03	$\log k_{GE}^{E}$	4.26 ±0.04
$\log k_{EE'}^{N}$	7.38 ±0.03	$\log k_{EE'}^{G}$	3.70 ±0.03	$\log k_{GE}^{E'}$	4.26 ±0.04
$\log k_{NGG'}^{N'}$	8.91 ±0.01	**$\log k_{NN'G}^{G'}$**	**3.45 ±0.01**	**$\log k_{NN'G}^{E}$**	**2.31 ±0.02**
$\log k_{NGE'}^{N'}$	7.16 ±0.02	**$\log k_{NN'E}^{G}$**	**3.48 ±0.01**	**$\log k_{NN'G}^{E'}$**	**2.31 ±0.02**
$\log k_{NG'E'}^{N'}$	7.14 ±0.03	**$\log k_{NN'E}^{G'}$**	**3.48 ±0.01**	**$\log k_{NN'E}^{E'}$**	**2.34 ±0.02**
$\log k_{NG'E}^{N'}$	8.99 ±0.03	$\log k_{NGE'}^{G'}$	3.52 ±0.03	$\log k_{NGG'}^{E}$	2.30 ±0.03
$\log k_{NEE'}^{N'}$	7.24 ±0.03	$\log k_{NG'E}^{G}$	3.49 ±0.03	$\log k_{NGG'}^{E'}$	4.13 ±0.02
$\log k_{NGE}^{N'}$	9.02 ±0.02	$\log k_{NG'E}^{G}$	3.49 ±0.03	$\log k_{NGE}^{E}$	2.33 ±0.03
$\log k_{GG'E}^{N}$	7.15 ±0.01	$\log k_{NEE'}^{G}$	3.52 ±0.03	$\log k_{NG'E'}^{E}$	2.33 ±0.03
$\log k_{GG'E}^{N'}$	8.98 ±0.01	$\log k_{NEE'}^{G'}$	3.55 ±0.03	$\log k_{NG'E}^{E'}$	4.16 ±0.02
$\log k_{GEE'}^{N}$	7.20 ±0.02	$\log k_{NGE}^{G'}$	3.52 ±0.03	$\log k_{NGE}^{E'}$	4.16 ±0.02
$\log k_{GEE'}^{N'}$	7.23 ±0.02	$\log k_{GEE'}^{G'}$	3.56 ±0.03	$\log k_{GG'E}^{E'}$	4.15 ±0.04
$\log k_{NGG'E}^{N'}$	8.84 ±0.01	**$\log k_{NN'GE}^{G'}$**	**3.34 ±0.02**	**$\log k_{NN'GG'}^{E}$**	**2.20 ±0.02**
$\log k_{NGG'E'}^{N'}$	6.98 ±0.01	**$\log k_{NN'GE'}^{G'}$**	**3.34 ±0.02**	**$\log k_{NN'GE}^{E'}$**	**2.23 ±0.02**
$\log k_{NGEE'}^{N'}$	7.09 ±0.02	**$\log k_{NN'EE'}^{G}$**	**3.37 ±0.02**	**$\log k_{NN'GE}^{E}$**	**2.23 ±0.02**
$\log k_{NG'EE'}^{N'}$	7.06 ±0.02	$\log k_{NGEE'}^{G'}$	3.41 ±0.03	$\log k_{NGG'E}^{E}$	4.05 ±0.03
$\log k_{GG'EE'}^{N}$	7.05 ±0.01	$\log k_{NG'EE'}^{G}$	3.38 ±0.03	$\log k_{NGG'E}^{E}$	2.22 ±0.03
$\log k_{NGG'EE'}^{N'}$	6.91 ±0.01	**$\log k_{NN'GEE'}^{G'}$**	**3.23 ±0.02**	**$\log k_{NN'GG'E}^{E'}$**	**2.12 ±0.03**
Interactivity parameters					
$\log\Delta E_{N/E}$	1.93 ±0.01*	$\log\Delta E_{N/G'}$	0.15 ±0.02	$\log\Delta E_{G/E'}$	0.11 ±0.01
$\log\Delta E_{N/G}$	0.18 ±0.02*	$\log\Delta E_{G/G'}$	0.14 ±0.01	$\log\Delta E_{N/E'}$	0.10 ±0.02
$\log\Delta E_{N/N'}$	0.16 ±0.02	$\log\Delta E_{G/E}$	0.11 ±0.01	$\log\Delta E_{E/E'}$	0.08 ±0.03

4.7 The microscopic protonation constants of ovothiol

The macroconstants of ovothiol were determined on the basis of ^{1}H NMR-pH titrations; the macroscopic protonation constants are as follows: $\log K_1$=10.21±0.03, $\log K_2$=8.63±0.04, $\log K_3$=2.02±0.06, $\log K_4$=0.95±0.07. For most molecules the chemical shift-pH profiles provide sufficient information to obtain the pH-dependent protonation percentage of the basic sites, and to quantitate the species-specific basicities by translating the experimental data into the relationships between the macro- and microconstants. However, these data are insufficient to determine the ovothiol microconstants, for the reasons below:

1. The number of basic sites exceeds three.

2. The proximity of the carbon-bound hydrogens and all proton-binding sites causes all the basic moieties to interact with one another and the NMR active hydrogens (i.e. the protonation of each site affects the basicity of all other basic moieties, and the chemical shift of all carbon-bound hydrogens).

3. Ovothiol has no molecular symmetry element(s) that would reduce the number of nonequivalent microspecies and simplify the evaluation.

4. Inherent basicities of the imidazole and amino sites highly exceed those of the thiolate and carboxylate sites, causing two practically separate, but pairwise overlapping protonation pH regions, and rendering half of the microspecies to be orders of magnitude smaller.

To elucidate the entire microspeciation of ovothiol, a combination of NMR-pH titrations and a deductive method were designed. Derivative molecules that are the possible closest models of the minor microscopic species were synthesized: ovothiol amide, *S*-methylovothiol, and *S*-methylovothiol amide.

In the major protonation pathways of ovothiol, first the imidazole and amino groups protonate in an overlapping fashion, next the carboxylate and thiolate groups protonate. In order to determine the species-specific protonation constants of the major microspeciation pathways, ^{1}H NMR-pH titrations were used, along with Sudmeier-Reilly type evaluation [71-72] equations. Based on the work of Sudmeier and Reilly

protonation shifts brought about the protonation of multiple basic sites simultaneously can be broken down as the sum of the individual standard protonation shifts weighed according to the degree of protonation as follows:

$$\Delta\delta_{\text{obs}}^{\text{Im2H}}(\text{pH}) = \chi_{\text{Im}}\Delta\delta_{\text{Im/Im2H}} + \chi_{\text{N}}\Delta\delta_{\text{N/Im2H}} \tag{30}$$

$$\Delta\delta_{\text{obs}}^{\alpha\text{H}}(\text{pH}) = \chi_{\text{Im}}\Delta\delta_{\text{Im/}\alpha\text{H}} + \chi_{\text{N}}\Delta\delta_{\text{N/}\alpha\text{H}} \tag{31}$$

where $\Delta\delta_{\text{obs}}^{\text{Im2H}}(\text{pH})$ and $\Delta\delta_{\text{obs}}^{\alpha\text{H}}(\text{pH})$ are the pH-dependent observed protonation shifts of ovothiol (the observed chemical shift at a particular pH minus the observed chemical shift at high pH where the molecule is in its completely basic form) at the imidazole C2 and aliphatic α hydrogens, respectively. x_{Im} and x_{N} are the pH-dependent degrees of protonation at the respective imidazole and amino sites in ovothiol, $\Delta\delta^{\text{Im/Im2H}}$, $\Delta\delta^{\text{N/Im2H}}$, $\Delta\delta^{\text{Im/}\alpha\text{H}}$ and $\Delta\delta^{\text{N/}\alpha\text{H}}$ are the pH-independent, standard chemical shift changes at the imidazole C2 and α hydrogens, brought about by the complete protonation of the imidazole and amino sites. Standard protonation shifts quantitate to what extent and direction the protonation of a particular basic site modifies the chemical shift of the observed, respective, carbon-bound imidazole C2 or aliphatic α hydrogen. These four standard protonation shift values could be obtained from the *S*-methylovothiol titration, where the amino and imidazole sites protonate in separate steps. Since the x_{Im} and x_{N} functions, the degree of protonation take on 1 as upper limiting value upon complete protonation, the maximum values of the observed protonation shifts are:

$$\Delta\delta_{\text{obs}}^{\text{Im2H}}(\text{max}) = \Delta\delta^{\text{Im/Im2H}} + \Delta\delta^{\text{N/Im2H}} \tag{32}$$

$$\Delta\delta_{\text{obs}}^{\alpha\text{H}}(\text{max}) = \Delta\delta^{\text{Im/}\alpha\text{H}} + \Delta\delta^{\text{N/}\alpha\text{H}} \tag{33}$$

Even though *S*-methylovothiol is the closest possible model for the S-protonated ovothiol, the protonation shift at any carbon-bound hydrogen in *S*-methylovothiol will not add up exactly to the respective protonation shift change in ovothiol. The $\Delta\delta_{obs}^{Im2H}(max)$ and $\Delta\delta_{obs}^{\alpha H}(max)$ values of *S*-methylovothiol have therefore been normalized to that of ovothiol by proportionally multiplying them by a number slightly different from unity [73-74].

The k^{Im} and k^{N} protonation microconstants are involved in the x_{Im} and x_{N} (pH-dependent degrees of protonation) functions. We therefore express the x values in terms of these microspecies, the related microconstants and hydrogen ion concentrations, as follows:

$$\chi_{Im} = \frac{[b]+[f]}{[a]+[b]+[c]+[f]} = \frac{k^{Im}[H^+]+\beta_2[H^+]^2}{1+\beta_1[H^+]+\beta_2[H^+]^2} \tag{34}$$

$$\chi_{N} = \frac{[c]+[f]}{[a]+[b]+[c]+[f]} = \frac{k^{N}[H^+]+\beta_2[H^+]^2}{1+\beta_1[H^+]+\beta_2[H^+]^2} \tag{35}$$

By fitting the curves of equations (34) and (35) on the titration data of ovothiol we obtained the k^{Im} and k^{N} values of ovothiol. The remaining microconstants of the major pathways were calculated with the interactivity parameter between the imidazole and amino groups.

The chemical shift change of the α and imidazole 2H protons perturbed by the carboxylate and thiolate groups could also be calculated, using the standard chemical shift change values observed in *S*-methylovothiol (where only the carboxylate moiety is protonated) and ovothiol amide (where only the thiolate group is protonated) respectively, with a similar method as described above, using Sudmeier-Reilly type equations, along with the aforementioned relationships between the macro- and microconstants.

Since there are two distinct protonation pH regions in ovothiol, the α and imidazole 2H chemical shift changes perturbed by the carboxylate and thiolate groups could also be

calculated, using the standard chemical shift change values of *S*-methylovothiol and ovothiol amide respectively with a similar method as described previously. The microscopic protonation constants of the aforementioned derivative compounds (OvSMe, OvSHAmide, OvSMeAmide) were considered to be constituent microconstants in the microspeciation of ovothiol. The remaining microconstants were calculated using the determined interactivity parameters, the relationships between the macro- and microconstants. The complete set of ovothiol microconstants, interactivity parameters and protonation shifts are compiled in Tables 7 and 8. The results above were confirmed with complementary experiments and evaluations, carried out with three independent techniques: *S*-methyl ^{1}H NMR-pH titration of S-methylovothiol amide, UV-pH titration of *S*-methylovothiol amide, and ^{15}N NMR-pH titration of ovothiol.

Table 7 The species-specific protonation microconstants (298 K, 0.15 mol/L ionic strength) in log values and standard ^{1}H NMR protonation shifts in ppm of ovothiol ±s.d.

Imidazole		Amino		Carboxylate		Thiolate	
symbol	**value**	**symbol**	**value**	**symbol**	**value**	**symbol**	**value**
OvSH Microscopic protonation constants							
$\log k^{\mathrm{Im}}$	10.07 ±0.01	$\log k^{\mathrm{N}}$	9.85 ±0.01	$\log k^{\mathrm{O}}$	4.38 ±0.08	$\log k^{\mathrm{S}}$	6.34 ±0.08
$\log k_{\mathrm{N}}^{\mathrm{Im}}$	8.99 ±0.05	$\log k_{\mathrm{Im}}^{\mathrm{N}}$	8.78 ±0.05	$\log k_{\mathrm{Im}}^{\mathrm{O}}$	3.7 ±0.1	$\log k_{\mathrm{Im}}^{\mathrm{S}}$	2.8 ±0.2
$\log k_{\mathrm{O}}^{\mathrm{Im}}$	9.43 ±0.01	$\log k_{\mathrm{O}}^{\mathrm{N}}$	8.05 ±0.06	$\log k_{\mathrm{N}}^{\mathrm{O}}$	2.6 ±0.1	$\log k_{\mathrm{N}}^{\mathrm{S}}$	4.9 ±0.1
$\log k_{\mathrm{S}}^{\mathrm{Im}}$	6.5 ±0.1	$\log k_{\mathrm{S}}^{\mathrm{N}}$	8.4 ±0.1	$\log k_{\mathrm{S}}^{\mathrm{O}}$	4.13 ±0.02	$\log k_{\mathrm{O}}^{\mathrm{S}}$	6.10 ±0.02
$\log k_{\mathrm{ON}}^{\mathrm{Im}}$	8.35 ±0.05	$\log k_{\mathrm{OIm}}^{\mathrm{N}}$	6.97 ±0.03	$\log k_{\mathrm{NIm}}^{\mathrm{O}}$	1.93 ±0.09	$\log k_{\mathrm{NIm}}^{\mathrm{S}}$	1.3 ±0.1
$\log k_{\mathrm{SN}}^{\mathrm{Im}}$	5.4 ±0.1	$\log k_{\mathrm{SIm}}^{\mathrm{N}}$	7.3 ±0.1	$\log k_{\mathrm{SIm}}^{\mathrm{O}}$	3.4 ±0.1	$\log k_{\mathrm{OIm}}^{\mathrm{S}}$	2.47 ±0.07
$\log k_{\mathrm{SO}}^{\mathrm{Im}}$	5.80 ±0.07	$\log k_{\mathrm{SO}}^{\mathrm{N}}$	6.62 ±0.02	$\log k_{\mathrm{SN}}^{\mathrm{O}}$	2.4 ±0.1	$\log k_{\mathrm{ON}}^{\mathrm{S}}$	4.67 ±0.06
$\log k_{\mathrm{SON}}^{\mathrm{Im}}$	4.72 ±0.02	$\log k_{\mathrm{SOIm}}^{\mathrm{N}}$	5.54 ±0.07	$\log k_{\mathrm{SNIm}}^{\mathrm{O}}$	1.69 ±0.03	$\log k_{\mathrm{ONIm}}^{\mathrm{S}}$	1.04 ±0.03
OvSH Species-specific protonation shifts							
$\Delta\delta_{\mathrm{Im/Im2H}}$	0.84 ±0.01	$\Delta\delta_{\mathrm{N/Im2H}}$	0.045 ±0.001	$\Delta\delta_{\mathrm{O/Im2H}}$	0.040 ±0.002	$\Delta\delta_{\mathrm{S/Im2H}}$	0.464 ±0.005
$\Delta\delta_{\mathrm{Im/\alpha H}}$	0.053 ±0.003	$\Delta\delta_{\mathrm{N/\alpha H}}$	0.534 ±0.009	$\Delta\delta_{\mathrm{O/\alpha H}}$	0.50 ±0.01	$\Delta\delta_{\mathrm{S/\alpha H}}$	-0.155 ±0.007

Table 8. Interactivity parameters in ovothiol in log values ±s.d.

Interactivity parameters

$\log\Delta E_{Im/N}$	1.08 ±0.05
$\log\Delta E_{N/O}$	1.85 ±0.05
$\log\Delta E_{Im/O}$	0.70 ±0.05
$\log\Delta E_{N/S}$	1.43 ±0.06
$\log\Delta E_{Im/S}$	3.63 ±0.07
$\log\Delta E_{O/S}$	0.24 ±0.08

4.8 The microscopic protonation constants of ovothiol disulfide

The macroscopic protonation constants of ovothiol disulfide were determined using simultaneous regression analysis on the potentiometric and ^{1}H NMR-pH titration data. The macroscopic protonation constant values and titration curves indicate the amino moieties protonate in an overlapping fashion followed largely separately by the overlapping protonation of the carboxylate and imidazole moieties, thus forming two practically separate protonation pH regions.

Table 9. The macroscopic protonation constants of ovothiol disulfide (OvSSOv) and related compounds (298 K, 0.15 mol/L ionic strength) in log values ±s.d. Abbreviation of the related model compounds: ovothiol disulfide methyl ester (OvOMeSSOv), ovothiol disulfide dimethyl ester (OvOMeSSOvOMe).

	OvSSOv	OvOMeSSOv	OvOMeSSOvOMe
$\log K_1$	9.05 ±0.02	8.56 ±0.01	7.18 ±0.01
$\log K_2$	8.22 ±0.01	6.69 ±0.01	6.22 ±0.01
$\log K_3$	4.87 ±0.01	4.24 ±0.02	3.87 ±0.02
$\log K_4$	3.01 ±0.02	2.78 ±0.02	1.96 ±0.02
$\log K_5$	2.37 ±0.03	1.82 ±0.02	-
$\log K_6$	1.65 ±0.02	-	-

At basic pH, the two amino moieties of ovothiol disulfide are primarily protonated. Due to symmetry, the relationships between the first two macroscopic protonation constants and the major amino microscopic protonation constants become:

$$\log k^{\mathrm{N}} = \log K_1 - \log 2 \qquad (36)$$

$$\log k_{\mathrm{N}}^{\mathrm{N'}} = \log K_2 + \log 2 \qquad (37)$$

The difference of the above microscopic protonation constants also afforded the opposite-side amino interactivity parameter $\log\Delta E_{\mathrm{N/N'}}$. The entire set of the microscopic protonation constants and interactivity parameters are compiled in Table 10 and Table 11, respectively.

Table 10. The species-specific protonation constants (298 K, 0.15 mol/L ionic strength) of ovothiol disulfide in log values ±s.d. The microconstants of the major pathway are in bold.

Microscopic protonation constants					
Amino		Imidazole		Carboxylate	
symbol	value ±s.d.	symbol	value ±s.d.	symbol	value ±s.d.
$\log k^{N}$	**8.75 ±0.02**	$\log k^{Im}$	6.6 ±0.1	$\log k^{O}$	5.08 ±0.09
$\log k_{N}^{N'}$	**8.52 ±0.01**	$\log k_{N}^{Im'}$	5.65 ±0.05	$\log k_{N}^{O'}$	4.91 ±0.06
$\log k_{Im}^{N'}$	7.8 ±0.1	$\log k_{N}^{Im}$	5.5 ±0.1	$\log k_{N}^{O}$	3.23 ±0.07
$\log k_{Im}^{N}$	7.67 ±0.05	$\log k_{Im}^{Im'}$	5.3 ±0.1	$\log k_{Im}^{O'}$	4.78 ±0.09
$\log k_{O}^{N'}$	8.58 ±0.06	$\log k_{O}^{Im'}$	6.3 ±0.1	$\log k_{Im}^{O}$	4.4 ±0.1
$\log k_{O}^{N}$	6.90 ±0.05	$\log k_{O}^{Im}$	5.9 ±0.1	$\log k_{O}^{O'}$	5.03 ±0.09
$\log k_{NIm'}^{N'}$	7.44 ±0.05	$\log k_{NN'}^{Im}$	**4.57 ±0.01**	$\log k_{NN'}^{O}$	**3.06 ±0.04**
$\log k_{NIm}^{N'}$	7.6 ±0.1	$\log k_{NIm'}^{Im}$	4.2 ±0.1	$\log k_{NIm'}^{O'}$	4.21 ±0.08
$\log k_{NO}^{N'}$	6.67 ±0.06	$\log k_{NIm}^{Im'}$	4.34 ±0.08	$\log k_{NIm}^{O}$	2.93 ±0.08
$\log k_{NO'}^{N'}$	8.35 ±0.06	$\log k_{NO'}^{Im}$	5.2 ±0.1	$\log k_{NIm'}^{O}$	4.61 ±0.07
$\log k_{ImIm'}^{N}$	6.7 ±0.1	$\log k_{NO}^{Im'}$	4.9 ±0.1	$\log k_{NIm}^{O}$	2.53 ±0.09
$\log k_{ImO'}^{N}$	7.50 ±0.08	$\log k_{NO}^{Im'}$	5.35 ±0.06	$\log k_{NO}^{O}$	3.18 ±0.08
$\log k_{ImO'}^{N'}$	5.97 ±0.09	$\log k_{NO}^{Im}$	4.8 ±0.1	$\log k_{NO}^{O'}$	4.86 ±0.07
$\log k_{ImO}^{N'}$	7.65 ±0.08	$\log k_{ImO'}^{Im'}$	4.6 ±0.1	$\log k_{ImIm'}^{O}$	4.1 ±0.1
$\log k_{ImO}^{N}$	5.82 ±0.07	$\log k_{ImO}^{Im'}$	5.0 ±0.1	$\log k_{ImO}^{O}$	4.33 ±0.09
$\log k_{OO'}^{N}$	6.88 ±0.01	$\log k_{OO'}^{Im}$	5.6 ±0.1	$\log k_{ImO}^{O'}$	4.6 ±0.1
$\log k_{NImIm'}^{N'}$	6.5 ±0.1	$\log k_{NN'Im}^{Im'}$	**3.26 ±0.06**	$\log k_{NN'Im}^{O}$	**2.36 ±0.06**
$\log k_{NImO}^{N'}$	5.74 ±0.08	$\log k_{NN'O}^{Im}$	**3.87 ±0.08**	$\log k_{NN'Im}^{O'}$	**2.76 ±0.05**
$\log k_{NIm'O}^{N'}$	5.59 ±0.07	$\log k_{NN'O}^{Im'}$	**4.27 ±0.03**	$\log k_{NN'O}^{O'}$	**3.01 ±0.04**
$\log k_{NIm'O}^{N'}$	7.27 ±0.08	$\log k_{NImO'}^{Im'}$	3.64 ±0.06	$\log k_{NImIm'}^{O}$	2.23 ±0.09
$\log k_{NOO'}^{N'}$	6.52 ±0.01	$\log k_{NIm'O}^{'Im}$	3.9 ±0.1	$\log k_{NImIm'}^{O'}$	3.91 ±0.09
$\log k_{NImO}^{N'}$	7.42 ±0.07	$\log k_{NIm'O}^{Im}$	3.5 ±0.1	$\log k_{NImO}^{O}$	2.48 ±0.07
$\log k_{ImIm'O}^{N}$	4.9 ±0.1	$\log k_{NOO'}^{Im}$	4.65 ±0.06	$\log k_{NIm'O}^{O'}$	2.7 ±0.1
$\log k_{ImIm'O}^{N'}$	6.57 ±0.09	$\log k_{NOO'}^{Im'}$	4.65 ±0.06	$\log k_{NIm'O}^{O'}$	4.16 ±0.06
$\log k_{ImOO'}^{N}$	5.80 ±0.05	$\log k_{NImO}^{Im'}$	4.04 ±0.07	$\log k_{NImO}^{O'}$	4.4 ±0.1
$\log k_{ImOO'}^{N'}$	5.80 ±0.06	$\log k_{ImOO'}^{Im'}$	4.3 ±0.1	$\log k_{ImIm'O}^{O'}$	4.0 ±0.1
$\log k_{NImIm'O}^{N'}$	6.34 ±0.09	$\log k_{NN'ImO}^{Im'}$	**2.96 ±0.05**	$\log k_{NN'ImIm'}^{O}$	**2.06 ±0.06**
$\log k_{NImIm'O'}^{N'}$	4.7 ±0.1	$\log k_{NN'ImO'}^{Im'}$	**2.56 ±0.08**	$\log k_{NN'ImO}^{O'}$	**2.56 ±0.04**
$\log k_{NImOO'}^{N'}$	5.57 ±0.06	$\log k_{NN'OO'}^{Im}$	**3.57 ±0.02**	$\log k_{NN'ImO}^{O}$	**2.31 ±0.04**
$\log k_{NIm'OO'}^{N'}$	5.4 ±0.1	$\log k_{NImOO'}^{Im'}$	3.34 ±0.05	$\log k_{NImIm'O}^{O'}$	3.86 ±0.07
$\log k_{ImIm'OO'}^{N}$	4.72 ±0.08	$\log k_{NIm'OO'}^{Im}$	3.2 ±0.1	$\log k_{NImIm'O'}^{O}$	2.18 ±0.08
$\log k_{NImIm'OO'}^{N'}$	4.49 ±0.07	$\log k_{NN'ImOO'}^{Im'}$	**2.26 ±0.02**	$\log k_{NN'ImIm'O}^{O'}$	**2.01 ±0.05**

Table 11. The interactivity parameters of ovothiol disulfide in log values ±s.d.

Interactivity parameters					
$\log\Delta E_{N/N'}$	0.23 ±0.02	$\log\Delta E_{Im/Im'}$	1.31 ±0.03	$\log\Delta E_{O/O'}$	0.1 ±0.1
$\log\Delta E_{N/Im}$	1.08 ±0.05	$\log\Delta E_{Im/N'}$	0.9 ±0.1	$\log\Delta E_{O/N'}$	0.17 ±0.06
$\log\Delta E_{O/N}$	1.85 ±0.05	$\log\Delta E_{O/Im}$	0.70 ±0.05	$\log\Delta E_{O/Im'}$	0.30 ±0.03

At acidic pH the overlapping protonation of the remaining four basic moieties predominates. To untangle the species-specific protonation constants of the carboxylate and imidazole moieties, two newly synthesized auxiliary model compounds were used. Ovothiol disulfide dimethyl ester (OvOMeSSOvOMe) is the closest mimic of the microspecies protonated at both carboxylates. Thus, the protonation constants of this compound can be regarded as constituents of the ovothiol disulfide microspeciation scheme. After the ^{1}H NMR-pH titration of ovothiol disulfide dimethyl ester a basic solution of this compound was titrated: in the course of titration ester hydrolysis occurred and ovothiol disulfide dimethyl ester, ovothiol disulfide methyl ester (OvOMeSSOv), and ovothiol disulfide were formed. However, because unique signals were available for each of these species in the NMR spectra, their protonation constants could be measured in parallel with the parent compound values. The relationships between the macro- and microconstants afforded the remaining microconstants and opposite-side imidazole-imidazole interactivity parameter. The interactivity parameter between the carboxylate and imidazole groups residing on the same half of the molecule ($\log\Delta E_{O/N}$) could be imported from the microspeciation of ovothiol, since analogous moieties in ovothiol and ovothiol disulfide can be assumed to interact similarly.

4.9 The microscopic protonation constants of lipoic acid and its derivatives

Lipoic acid, dihydrolipoic acid, lipoamide, and dihydrolipoamide were titrated under near physiological conditions. The macroscopic protonation constants are compiled in Table 12. Lipoamide was only titrated to demonstrate the effect of deprotonation of the amide group. Because of the complexity of the proton spectra, in addition to ^{1}H NMR-pH titration, ^{1}H/^{13}C HSQC-pH titrations were also performed with dihydrolipoic acid, to aid the chemical shift assessment. Dihydrolipoamide was chosen as the appropriate

model compound sufficient to elucidate the triprotic system of dihydrolipoic acid, since appropriately chosen NMR nuclei can provide selective signals of the mid-chain thiolate, both for dihydrolipoic acid and dihydrolipoamide. The titration curves of lipoic acid revealed that the protonation shift decreases drastically as the covalent distance increases between the observed proton and the basic moiety: $\Delta\delta_{C2}=0.218 \pm0.002$, $\Delta\delta_{C3}=0.046 \pm0.002$, $\Delta\delta_{C4}=0.038 \pm0.002$, $\Delta\delta_{C5}=0.003 \pm0.002$. In fact, reasonable titration curves could not be fitted to the chemical shifts of the C6, C7, and C8 hydrogens. Therefore it is safe to assume, that in the case of dihydrolipoic acid and dihydrolipoamide the C3 and C2 hydrogens will be selective for the S6 moiety of the two thiolates. The C3 protons are, in fact, the best-conditioned protons for the evaluation of the S6 thiolate basicities, since apart from selectivity they also have sufficient sensitivity for the mid-chain thiolate protonation. Therefore, the titration data of dihydrolipoamide was evaluated as such: the C6, C7a, and C8 hydrogen chemical shifts were fitted using equation (15), while simultaneously, the C3 proton chemical shifts were fitted to the following equation:

$$\delta_{obs}(pH) = \frac{(\delta_{HL} - \delta_L)(10^{\log k_O^{S6} - pH} + 10^{\log \beta_2 - 2pH})}{1 + 10^{\log \beta_1 - pH} + 10^{\log \beta_2 - 2pH}} + \delta_L \qquad (38)$$

where δ_L is the C3 chemical shift of the unprotonated dihydrolipoamide, δ_{HL} is the C3 chemical shift of the dihydrolipoamide species protonated at S6, β_1 and β_2 are the cumulative macroconstants of dihydrolipoamide. The chemical shift-pH profile of lipoamide revealed that the protonation shift due to deprotonation of the amide moiety does not perturb the C3 chemical shift considerably in dihydrolipoamide up to pH 13.5 (our region of interest). The remaining dihydrolipoamide microconstants could be calculated with equations analogous to equations (9) and (11). The titration data of dihydrolipoic acid were evaluated analogously: utilizing only the first two macroconstants, the C6, C7a (^{1}H and ^{13}C), and C8 chemical shifts were fitted to equation (15), while simultaneously, the C2 (^{1}H and ^{13}C) and C3 chemical shifts were fitted to the following function:

$$\delta_{obs}(pH) = \frac{(\delta_{HL} - \delta_L)(10^{\log k^{S6} - pH} + 10^{\log \beta_2 - 2pH}) + (\delta_{H_2L} - \delta_L)10^{\log \beta_3 - 3pH}}{1 + 10^{\log \beta_1 - pH} + 10^{\log \beta_2 - 2pH} + 10^{\log \beta_3 - 3pH}} + \delta_L \quad (39)$$

where δ_L is the chemical shift (C2, C3) of the unprotonated dihydrolipoic acid, δ_{HL} is the chemical shift (C2, C3) of the dihydrolipoic acid species where S6 is protonated and O is unprotonated, δ_{H2L} is the chemical shift (C2, C3) of the dihydrolipoic acid species where S6 and O are protonated, β_1, β_2 and β_3 are the cumulative protonation macroconstants of dihydrolipoic acid. The ^{13}C chemical shifts of the C7 carbon were chosen, because this nucleus is the most sensitive to the protonation of both thiolate moieties. Protonation of the thiolates and the carboxylate take place in separate pH regions, the K_3 and k_{S6S8}^O values of dihydrolipoic acid are therefore practically identical. The remaining microconstants of dihydrolipoic acid could be calculated with equations analogous to equations (9) and (11). All macro- and microconstants and interactivity parameters of dihydrolipoic acid are presented in Table 12 and 13.

Table 12. The macroscopic protonation constants of lipoic acid, dihydrolipoic acid, and dihydrolipoamide (298 K, 0.15 mol/L ionic strength) in log values ±s.d.

	Lipoic acid	Dihydrolipoic acid	Dihydro-lipoamide
$\log K_1$	4.65 ±0.01	11.17 ±0.01	11.05 ±0.02
$\log K_2$	-	9.79 ±0.03	9.69 ±0.03
$\log K_3$	-	4.64 ±0.01	-

Table 13. The microscopic protonation constants (298 K, 0.15 mol/L ionic strength) and interactivity parameters of dihydrolipoic acid in log values ±s.d.

Microscopic protonation constants					
mid-chain thiolate (S6)		end-chain thiolate (S8)		carboxylate (O)	
symbol	value	symbol	value	symbol	value
$\log k^{S6}$	10.97 ±0.01	$\log k^{S8}$	10.74 ±0.03	$\log k^{O}$	4.87 ±0.05
$\log k_{S8}^{S6}$	10.23 ±0.04	$\log k_{S6}^{S8}$	9.99 ±0.03	$\log k_{S6}^{O}$	4.74 ±0.05
$\log k_{O}^{S6}$	10.85 ±0.01	$\log k_{O}^{S8}$	10.62 ±0.06	$\log k_{S8}^{O}$	4.76 ±0.01
$\log k_{S8O}^{S6}$	10.12 ±0.07	$\log k_{S6}^{S8}$	9.89 ±0.04	$\log k_{S6S8}^{O}$	4.64 ±0.01
Interactivity parameters					
$\log\Delta E_{S6/S8}$	0.74 ±0.04	$\log\Delta E_{S6/O}$	0.12 ±0.01	$\log\Delta E_{S8/O}$	0.10 ±0.05
$\log\Delta E_{S6/S8}$	0.73 ±0.07	$\log\Delta E_{S6/O}$	0.10 ±0.08	$\log\Delta E_{S8/O}$	0.12 ±0.06

4.10 Determining species-specific redox equilibrium constants and standard redox potentials

For the thiol-disulfide redox equilibria, only the apparent or conditional equilibrium constants (K_{3C}) are directly available, by determining the equilibrium concentrations of RSH, GSSG, RSSR, and GSH in the reaction mixtures. The conditional equilibrium constants were calculated from the concentrations in the equilibrium reaction mixtures according to equation (3). The conditional redox equilibrium constant values are listed in Table 14.

Table 14. The conditional redox equilibrium constants of cysteamine-, cysteine-, homocysteine-, penicillamine-, ovothiol-glutathione thiol-disulfide systems. The uncertainties in the pH and $\log K_{3C}$ values are 0.01-0.02 and 0.002-0.004, respectively.
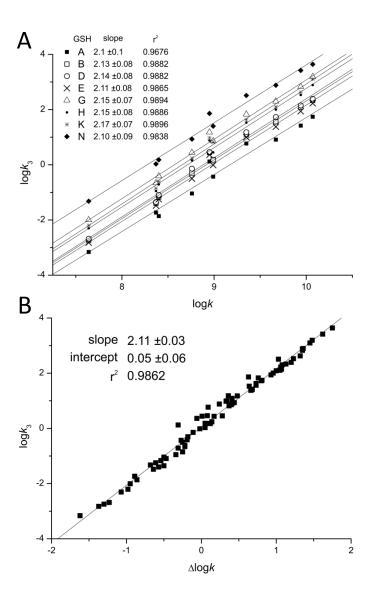
Cysteamine		Cysteine		Homocysteine		Penicillamine		Ovothiol	
pH	$\log K_{3C}$	pH	$\log K_{3C}$	pH	$\log K_{3C}$	pH	$\log K_{3C}$	pH	$\log K_{3C}$
0.99	-0.154	0.86	0.028	0.91	0.099	0.84	-0.155	0.85	-0.850
1.31	-0.097	1.25	0.078	1.22	0.137	1.26	-0.119	1.24	-1.402
1.59	-0.071	1.54	0.113	1.54	0.203	1.52	-0.056	1.78	-2.444
1.83	-0.097	1.81	0.176	1.81	0.263	1.85	-0.027	2.43	-2.924
2.62	-0.222	2.61	0.197	2.61	0.335	2.31	-0.009	3.02	-3.889
2.93	-0.252	2.89	0.146	2.89	0.323	2.91	-0.086	4.11	-5.278
3.17	-0.260	3.20	0.122	3.20	0.288	3.25	-0.137	5.09	-5.793
3.95	-0.328	3.40	0.116	3.40	0.174	3.41	-0.237	5.61	-6.124
5.43	-0.319	5.60	-0.273	5.62	-0.051	5.54	-0.310	6.28	-5.875
6.55	-0.251	6.42	-0.230	6.37	-0.056	6.40	-0.328	7.21	-6.267
7.87	-0.495	7.67	-0.204	7.60	-0.092	7.67	-0.456	8.08	-5.851
7.92	-0.509	8.83	0.105	8.83	-0.048	8.88	-1.046	9.20	-5.412
9.62	-1.347	9.67	0.601	9.67	0.280	9.67	-0.745	9.42	-5.050
10.20	-0.523	9.98	0.779	9.98	0.693	9.90	-0.699	10.28	-4.611
10.60	0.021	10.44	1.244	10.44	1.003	10.44	-1.398	11.34	-3.972
11.44	0.701	11.86	1.668	11.86	1.443	11.88	0.161	11.95	-3.878

The microscopic redox equilibrium constants were calculated from the conditional equilibrium constants using analogous equations as equation (14). Obviously, the conditional equilibrium constants were measured at different pH media, all of which theoretically afford the same value for a certain microscopic equilibrium constant. However, each microscopic redox equilibrium constant was calculated at pH values where the corresponding equation (14) is well-conditioned, i.e. the mole fractions of the involved microspecies are near-maximal. For k_3^{bB} the optimal pH of determination are 5.60, 6.42, 7.67, 8.83 (see Table 14). The mean of the calculated microscopic redox equilibrium constants are listed in Table 15.

The correlation between the species-specific redox equilibrium constants (within each block of GSH microspecies) and the thiolate species-specific protonation constants of CysASH, CysSH, hCysSH is depicted in Figure 7A, while the correlation between the $\log k_3^{xY}$ and $\Delta \log k$ (the difference in species-specific protonation constants of the involved RSH and GSH thiolates) are depicted in Figure 7B.

Table 15. Species-specific redox equilibrium constants. The uncertainties in the $\log k_3$ values are 0.01-0.03.

		Cysteamine		Cysteine				Homocysteine				Penicillamine				Ovothiol							
Glutathione		-	N	-	N	O	NO	-	N	C	NO	-	N	O	NO	-	Im	N	O	ImN	ImO	NO	ImNO
		a	b	a	b	d	f	a	b	d	f	a	b	d	f	A	B	C	D	F	G	I	L
-	A	0.91	-1.73	1.74	-1.04	0.12	-3.16	1.42	-0.43	0.77	-1.86	0.19	-2.24	-1.40	-4.51	-5.26	-12.52	-7.65	-6.55	-17.26	-12.80	-9.82	-17.85
N	B	1.56	-1.40	2.33	-0.30	0.44	-2.74	2.09	0.19	1.09	-1.17	0.51	-1.90	-1.07	-4.21	-4.94	-12.13	-7.33	-6.22	-16.04	-12.42	-9.70	-16.71
G	D	1.73	-1.35	2.39	-0.14	0.46	-2.68	2.15	0.18	1.18	-1.09	0.57	-1.81	-1.06	-4.16	-4.88	-12.10	-7.25	-6.12	-17.12	-12.35	-9.54	-17.22
E	E	1.38	-1.48	2.23	-0.50	0.36	-2.82	1.94	-0.01	1.00	-1.25	0.43	-1.96	-1.16	-4.38	-5.02	-12.27	-7.44	-6.41	-17.02	-12.57	-9.88	-17.42
NG	G	2.30	-0.66	3.19	0.44	1.18	-2.00	2.83	0.86	1.83	-0.41	1.25	-1.15	-0.35	-3.49	-4.21	-11.45	-6.63	-5.48	-16.02	-11.76	-8.96	-16.24
NE	H	2.00	-0.95	2.89	0.16	0.88	-2.30	2.53	0.45	1.53	-0.71	0.95	-1.46	-0.67	-3.75	-4.50	-11.74	-6.96	-5.75	-16.35	-12.01	-9.06	-16.49
GE	K	2.10	-0.85	3.10	0.24	0.98	-2.20	2.63	0.82	1.63	-0.61	1.05	-1.39	-0.55	-3.69	-4.40	-11.62	-6.83	-5.65	-16.09	-11.92	-8.96	-16.35
NGE	N	2.88	0.03	3.64	0.93	1.86	-1.32	3.42	1.40	2.51	0.18	1.93	-0.43	0.32	-2.80	-3.52	-10.78	-5.92	-4.67	-15.34	-11.06	-8.28	-15.34

60

Figure 7. A: The correlation between species-specific redox equilibrium constants and the species-specific thiolate protonation constants. Each symbol represents the thiol-disulfide equilibria involving various thiol microspecies of cysteamine, cysteine, and homocysteine with a selected glutathione microspecies (A, B, D, E, G, H, K, N). B: The correlation between species-specific redox equilibrium constants ($\log k_3^{xY}$) and the difference between species-specific thiolate protonation constants of the involved RSH and GSH microspecies ($\Delta \log k$).

Determination of the redox potential of the GSSG/GSH system was achieved indirectly, applying a redox couple with a known standard redox potential. For this purpose the biologically ubiquitous NAD^+/NADH (or $NADP^+$/NADPH) system could be a straightforward choice. However, based on the structure and triprotic nature of NAD^+ it was anticipated that the protonation of these moieties will influence the already pH-dependent redox potential of the system. Based on preliminary results the chemical shift of the pyridinium ring-bound hydrogens vary greatly with the protonation of the basic moieties, therefore the electron density around the pyridinium ring is certainly perturbed. The redox behavior of the NAD^+/NADH system is therefore influenced by 1) the pH of the solution, since hydrogen ions participate in the redox half-reaction, 2) the 8 protonation states of NAD^+, due to its three basic moieties, 3) the 16 protonation states of NADH, due to its four basic moieties (two pyrophosphate moieties, an adenine ring, and an added dihydropyridine ring). Therefore, the simplest nicotinamide nucleotide analogue system, 1-methylnicotinamide (MNA^+, the oxidized form), and 1-methyldihydronicotinamide (MNAH, the reduced form) was used as comparison redox couple. MNAH can take part in A) acid-base and B) redox reactions.

A) The dihydropyridine ring of MNAH can protonate, described by the following chemical equilibrium, protonation constant, and law of conservation of mass:

$$MNAH + H^+ = HMNAH^+ \tag{40}$$

$$K = \frac{[HMNAH^+]}{[MNAH][H^+]} \tag{41}$$

$$[MNAH] + [HMNAH^+] = [MNAH_{Total}] \tag{42}$$

B) In redox reactions MNAH can be a two-electron reducing agent with the disulfide form of glutathione.

The K_C equilibrium constant of the redox reaction is a pH-dependent, conditional (apparent) one:

$$K_{\mathrm{C}} = \frac{[\mathrm{MNA}^+][\mathrm{GSH}]^2[\mathrm{H}^+]}{[\mathrm{MNAH_{Total}}][\mathrm{GSSG}]} \tag{43}$$

The oxidation and protonation of MNAH are interfering, codependent processes. We have therefore determined the protonation constant of MNAH by ^{1}H NMR-pH titration (Figure 8A). The resulting log$K$ value is 1.51 ±0.01, which indicates that MNAH exists in solution at pH>2.5 overwhelmingly in its neutral form. The electrode potential of the MNA$^+$/MNAH system was measured in a wide pH range against saturated calomel electrode, and then converted to redox potential values versus standard hydrogen electrode. In these measurements the MNA$^+$ and MNAH$_{\mathrm{Total}}$ concentrations were kept equal. The practical form of the Nernst equation (expressed with concentrations) for such a redox transition, where hydrogen ion also takes part in the reaction, is as follows:

$$E = E° + \frac{RT}{zF}\ln\frac{[\mathrm{MNA}^+][\mathrm{H}^+]}{[\mathrm{MNAH}]} \tag{44}$$

where R is the universal gas constant, T is the absolute temperature, z is the number of moles of electrons transferred in the half-reaction, and F is the Faraday constant. Based on the acid-base characterization of MANH, [MNAH] is practically equal to [MNAH$_{\mathrm{Total}}$] in the pH media where the electrode potentials were measured, thus equation (44) takes the simpler form:

$$E = E° + \frac{RT}{zF}\ln[\mathrm{H}^+] \tag{45}$$

Therefore, the linear regression analysis of these data afforded the standard redox potential as the intercept; $E°$(MNA$^+$/MNAH)=-194 ±2 mV (Figure 8B). Below this pH range however, the relative amount of [MNAH] decreases as it gradually protonates. In

such an experimental setting, where $[MNA^+]/[MNAH_{Total}]$ is constant but the Nernstian term $[MNA^+]/[MNAH]$ is changing, the theoretical curve of the electrode potential versus pH is given by the following function, as $[MNAH]$ can be expressed from equation (40):

$$E = E° + \frac{RT}{zF} \ln \frac{[MNA^+][H^+]}{[MNAH_{Total}]/(1+K[H^+])} \tag{46}$$

where K is the protonation constant of MNAH. Subsequently, since $[MNA^+]=[MNAH_{Total}]$ the above equation becomes:

$$E = E° + \frac{RT}{zF} \ln([H^+]+K[H^+]^2) \tag{47}$$

The curve of equation (47) is simulated on the redox potential data points (Figure 8B) to demonstrate the deviation of theoretical curve from linear occurring only below pH 2. The linear regression analysis is therefore certainly valid in attaining the standard redox potential.

For the redox equilibrium between MNAH and GSSG, only the apparent or conditional equilibrium constants (K_C) can be determined directly, by measuring the equilibrium concentrations of GSH, GSSG, MNA^+, and $MNAH_{Total}$ in the reaction mixtures, using quantitative ^{1}H NMR technique. These pH-dependent, conditional equilibrium parameters (compiled in Table 16, depicted in Figure 8C) consist of total concentrations of the involved species, since the integrals of the observed NMR signals correspond to the total concentration of a reactant or product macrospecies.

Determination of the k microscopic redox equilibrium constants from the K_C conditional equilibrium constants and related parameters is demonstrated below with the example of the k^B redox microconstant. Latter involves the B microspecies of reduced glutathione,

and the corresponding E' microspecies of glutathione disulfide and can be expressed in relation with the MNA$^+$/MNAH system by the following equation (in analogy to equation (15))

$$k^{\text{B}} = \frac{[\text{MNA}^+][\text{B}]^2[\text{H}^+]}{[\text{MNAH}][\text{E}']} = \frac{[\text{MNA}^+][\text{GSH}]^2 \chi_{\text{B}}^2[\text{H}^+]}{[\text{MNAH}_{\text{Total}}]\chi_{\text{MNAH}}[\text{GSSG}]\chi_{\text{E}'}} = K_{\text{C}} \frac{\chi_{\text{B}}^2}{\chi_{\text{MNAH}}\chi_{\text{E}'}} \qquad (48)$$

Thus, if K_{C}, the apparent equilibrium constant and the x values are known the k^{B} value and all the analogous, pH-independent, species-specific redox microconstants can be calculated. The species-specific standard redox potentials of the glutathione microspecies were calculated from the species-specific redox equilibrium constants using the Nernst equation, for example:

$$E^{\circ}{}_{\text{B}} = E^{\circ}{}_{\text{MNA}^+/\text{MNAH}} + \frac{RT}{zF} \ln k^{\text{B}} \qquad (49)$$
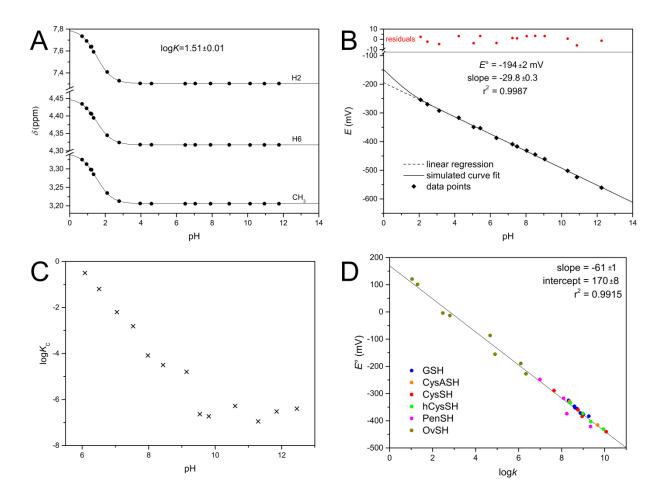
The species-specific standard redox potentials of the additional thiols were calculated using the species-specific redox equilibrium constants determined previously, and the standard redox potential of glutathione microspecies B, since it bears the least uncertainty. The means of the calculated species-specific standard redox potentials are listed in Table 17. The correlation between the species-specific standard redox potentials and the species-specific thiolate protonation constants is depicted in Figure 8D.

Table 16. Conditional redox equilibrium constants in log units of the reaction between MNA^+ and GSH. The uncertainties in the $\log K_C$ values are 0.02-0.04.

pH	$\log K_C$
6.08	-0.50
6.51	-1.21
7.04	-2.20
7.53	-2.82
7.98	-4.08
8.43	-4.50
9.14	-4.80
9.54	-6.64
9.81	-6.73
10.60	-6.28
11.30	-6.95
11.85	-6.52
12.46	-6.40

Table 17. Species-specific thiolate protonation constants and standard redox potentials of the corresponding thiol-disulfide systems. The one-letter symbols of microspecies are described in Figures 2-4. The uncertainties in the $E°$ values are 5-10 mV.

microspecies		$\log k$	$E°$ (mV)	microspecies		$\log k$	$E°$ (mV)
	A	9.26	-383		a	9.94	-431
	B	8.94	-374	hCysSH	b	8.99	-373
	D	8.87	-372		d	9.35	-403
	E	9.01	-376		f	8.4	-335
GSH	G	8.59	-346		a	9.34	-421
	H	8.71	-355	PenSH	b	8.09	-317
	K	8.62	-352		d	8.24	-374
	N	8.32	-325		f	6.99	-248
CysASH	a	9.67	-416		A	6.34	-227
	b	8.37	-329		B	2.8	-13
	a	10.07	-440		C	4.9	-155
	b	8.76	-360	OvSH	D	6.1	-189
CysSH	d	8.95	-384		F	1.3	101
	f	7.64	-289		G	2.47	-4
					I	4.67	-87
					L	1.04	121

Figure 8. A: The plot of ^{1}H chemical shifts versus pH for MNAH; dots are data points, solid lines are simulated curve fits. B: The pH dependence of the electrode potential (versus standard hydrogen electrode) of the MNA$^+$/MNAH redox couple. C: The pH dependence of the conditional redox equilibrium constant K_C (in log units) for the reaction between MNAH and GSSG. D: The correlation between species-specific standard redox potentials and the species-specific thiolate protonation constants for the various thiols.

5. DISCUSSION

The distinctive feature of cysteine among amino acids is its thiol group, an inherently weakly acidic moiety. The deprotonated, thiolate form occurs in physiological media infrequently only, but it is the reducing agent in redox equilibria, forming disulfides. A profound submolecular acid-base evaluation of thiol-containing amino acids and their disulfides facilitates deeper insight compared to the conventional macroscopic pKa values. Microspecies in the major protonation pathways certainly enjoy significant preference in abundance; however the minor pathways are also arranged hierarchically. In cysteine and homocysteine the monoprotonated microspecies are mainly b and c, while drastically smaller amount of d is present. The biprotonated ligand occurs mainly as e. Among the minor biprotonated microspecies, the one protonated at the thiolate and carboxylate groups is favored over the other minor microspecies. When the carboxylate-protonated microspecies takes on a second proton, the negatively charged thiolate is favored over the amino group, because the neighbor-group carboxylate protonation causes a stronger basicity-reducing effect on the adjacent amino than on the relatively remote thiolate. In the case of cystine and homocystine it is noteworthy that in the instance of biprotonated ligands (major microspecies: both amino groups protonated) the most favored minor microspecies is the one with opposite amino and cyrboxylate groups protonated, due to the Coulombic repulsion between hydronium ions and the ammonium ion, hence the opposite carboxylate will be slightly more basic. By far the least favored biprotonated species is the one whith both carboxylates protonated. Since hydrogen and sulfur are atoms of similar electronegativity, especially in the Mulliken-Jaffé scale, it is interesting to compare the amino and carboxylate basicities when either sulfhydryl (-SH) or disulfide (-S-S-) moieties are their neighbors. No or minor differences occur when the appropriate amino constants (logk_S^N of cysteine or homocysteine and logk^N of their disulfides) are compared.

Ovothiol, with a mere 24 atoms, but tetrafarious acid-base moieties and 32 protonation microconstants is one of the richest and most multifaceted chemical entities, if not the very richest among all the small biomolecules. The extremely rich functionality and the compact and corresponding electron system in ovothiol feature several peculiarities,

reflected by the microconstants. The $\log k^{Im}=10.07$ basicity is very high for an imidazole nitrogen, obviously due to the connected thiolate. On the other hand, the $\log k_{OSN}^{Im}=4.72$ value shows the strong impact of adjacent site protonations on the imidazole basicity. In fact, to our knowledge, the $\log\Delta E_{S/Im}=3.63$ interactivity parameter is the largest value of this kind among moieties of different type reported in any molecule. No doubt that the most interesting properties of ovothiol belong to the thiolate site. Even the highest thiolate basicity ($\log k^S=6.34$) is low for this type of moiety, reflecting the intramolecular electron-withdrawing effects of the surrounding imidazole and amino nitrogens and that of the carboxylate. The electron-withdrawing effects of these atoms/groups of inherently high electronegativity greatly increase upon protonation of these sites, resulting in the unprecedented low $\log k_{ONIm}^S=1.04$ value. This value is some 7 logk units smaller than the usual thiolate basicities, and also, it is even way below those observed in thioltransferase (GLRX glutaredoxin) enzymes [75-76], despite the fact that low thiolate basicity is a *sine qua non* property of thioltransferases.

The low thiolate basicity (i.e. high thiol acidity) of ovothiol renders this site to be anionic not only at basic, but also at the entire neutral, and even nearly throughout the acidic pH ranges. The "naked" thiolate form makes the molecule vulnerable to oxidation effects. This is most probably the reason why ovothiol has naturally been found under anaerobe conditions in deep seawater invertebrate eggs. The vulnerability to oxidation is, in turn, one of the most important preconditions of the antioxidant capacity. Since the surrounding amino, imidazole and carboxylate groups have been found to be more basic than the thiolate, and the 3 of these groups can be in a total of 2^3 protonation stages, the ovothiol sulfur atom occurs in solution in 8 differently modulated states of electron density. This provides high versatility in antioxidant capability within a single molecular skeleton.

The highly interwoven acid-base and redox properties of the GSH/GSSG-RSH/RSSR system can be decomposed into elementary, component equilibria if *a)* the species-specific protonation constants of GSH, GSSG, RSH, and RSSR are determined, and *b)* the conditional equilibrium constants of the pH-dependent redox equilibria are also quantified. As anticipated, the dissection of conditional equilibria into elementary redox ones in biological thiol-disulfide systems reveals significant differences between

reactions of apparently highly similar, covalently identical reactants, improving thus our understanding of redox homeostasis and providing new means to influence it. This is all the more important in light of the highly complex, parallel protonation equilibria of these multibasic biomolecules: not only the protonation of the thiolate, its protonation fraction, and the concomitant redox behavior will be very sensitive to minor pH changes, but the protonation state of neighboring basic moieties can influence the redox behavior by various inductive effects on the thiolate moiety. Major trends among the redox microconstants are that the values strictly increase as the strength and number of electron-withdrawing moieties increases on the glutathione species and vice versa on the thiol species. Such effects in the side-chain protonation are strongest in ovothiol (e.g. $k_3^{DN} >> k_3^{FA}$), due to the proximity and strong interaction of the imidazole moiety with the thiolate. Protonation of the ovothiol imidazole site decreases the k_3^{xY} value by a factor of 10^7, while protonation of the amino and carboxylate exert an effect of the same direction by a factor of 250 and 20, respectively. Effects of the glutathione side-chain protonation can be observed in columns downward as increasing $\log k_3^{xY}$ values. Even though in glutathione three groups protonate in the vicinity of its thiolate, their cumulative effect is typically less than 200 fold on the equilibrium constants. Upon comparing k_3^{AN} and k_3^{LA} ($10^{-3.52}$ and $10^{-17.85}$) in the ovothiol-glutathione system, the difference between these values is some 14 orders of magnitude, indicating that side-chain protonations can immensely modify thiol-disulfide equilibria, while covalent structures remain exactly the same.

The strong correlation between the species-specific thiolate protonation constants and species-specific redox equilibrium constants confirm the assumption that the thiol-disulfide redox reactions proceed via the thiolate form. As the electron density around the thiolate moiety increases, the proton binding affinity and oxidizability (inversely proportional to electron affinity) of the thiolate should increase proportionally, since both processes are governed by electron-density effects. The linear relationship between $\log k$ thiolate protonation microconstants and $\log k_3^{xY}$ redox equilibrium constants indicates that the acid-base and redox equilibria have been broken down to elementary reactions. The consistent slope of the correlation (mean value: 2.13 ±0.04) for the different thiol-disulfide equilibria involving various GSH microspecies also supports the hypothesis that these acid-base and redox processes are driven by the same force, and

the slope values are also in excellent agreement with the previous works of Keire *et al.* [16] (2.17 ±0.19) and Szajewski and Whitesides [30] (2.42). In Figure 7B all the data points align on the same line (slope: 2.11 ±0.03), with a very convincing linear regression going through the origin, indicating the presence of a collective fundamental process governing all thiol-disulfide transitions.

Concerning the standard redox potentials, the GSSG/GSH redox potential shows modest variability, owing to the relative remoteness between the sulfur and the other acid-base functions in the molecule. The highest thiolate oxidizability of GSH (-383 mV) belongs to the microspecies in which all other basic sites in the molecule are in non-protonated form. The easiest reducibility of GSSG (-325 mV) is borne by the microspecies of complete amino and carboxylate protonation. By far the greatest versatility can be observed on ovothiol, encompassing as many as 348 mV differences between its species-specific limiting redox potential values. This astonishing variability is due to the fact that the adjacent basic sites are in the close vicinity of the thiolate. While the ovothiol versatility way exceeds even the differences between extrema of any arbitrarily selected different molecules, the actual ovothiol values indicate apparently low intrinsic reducing capability of OvSH. The fact, however, that OvSH exists as thiolate nearly throughout the pH scale, makes ovothiol a promising antioxidant. The 30 standard redox potentials of the thiol-disulfide couples are determined for the first time; these values characterize the redox processes at the microspecies level.

6. CONCLUSIONS

The pH-dependent and species-selective equilibrium constants of the thiol-disulfide redox reactions between glutathione and important biogenic thiols were determined. The pH-independent species-specific redox equilibrium constant was implemented for the first time for thiol-disulfide systems; these values characterize the redox processes at the microspecies level. The different species-specific equilibrium constant values provide sound means to predict thiolate oxidizabilities, a key parameter to understand and influence oxidative stress. The standard redox potential values determined show close correlation with the respective thiolate basicities. The delicate task of medicinal antioxidants lies in their confinement: ROS (reactive oxygen species) surplus has to be eliminated, while physiological disulfides in proteins and peptides have to be kept intact. The major difficulty in designing effective antioxidants without decomposing the physiological disulfides in biomolecules is that the redox potential of the latter could not so far be determined. The correlation between the redox and acid-base properties serves now as a sound basis to quantify reducibility of disulfide moieties in physiological proteins and peptides, allowing thus the development of potent, selective antioxidant compounds.

7. SUMMARY

Species-specific standard redox potential of RSSR/RSH systems was determined to quantify thiol-disulfide equilibria of biological significance. The highly composite, codependent acid-base and redox equilibria of thiols could so far be converted into pH-dependent, apparent redox potentials (E'°) only. Since the formation of stable metal-thiolate complexes precludes the direct thiol-disulfide redox potential measurements by usual electrochemical techniques, an indirect method had to be elaborated. The species-specific, pH-independent standard redox potentials of glutathione were determined primarily by comparing it to 1-methylnicotinamide, the simplest NAD^+ analogue. The elucidation of the complete protonation microequilibria of the most important biogenic thiols and disulfides allowed the determination of species-specific standard redox potentials of the two-electron redox transitions of cysteamine, cysteine, homocysteine, penicillamine, ovothiol, and dihydrolipoic acid using their microscopic redox equilibrium constants with glutathione. The 30 different, microscopic standard redox potential values show close correlation with the respective thiolate basicities and provide sound means for the development of potent agents against oxidative stress.

8. ÖSSZEFOGLALÁS

Biológiailag nagy jelentőssęggel bíró tiol-diszulfid rendszerek részecske-specifikus standard redoxipotenciál értékeit határoztuk meg. A tiol-diszulfid rendszerek összetett és összefüggő sav-bázis és redoxi folyamatait mindezidáig csak pH-függő, látszólagos redoxipotentiállal ($E'°$) lehetett jellemezni. Mivel a tiolát ionok stabil komplexet képeznek minden fémfelületen a tiolok redoxipotenciálja nem határozható meg a hagyományos elektrokémiai módszerekkel, ezért egy közvetett módszer lett kifejlesztve a redoxipotenciálok meghatározására. Meghatároztuk a glutation részecske-specifikus, pH-független redoxi egyensúlyi állandóit 1-metilnikotinamiddal szemben, amely utóbbi vegyület a legegyszerűbb NAD^+ származék. A tiolok és diszulfidok teljes protonálódási mikrosémáinak valamint a glutationnal szembeni redoxi egyensúlyi állandóinak ismeretében meghatároztuk a legfontosabb tiolok – ciszteamin, cisztein, homocisztein, penicillamin, ovotiol, dihidroliponsav – részecske-specifikus standard redoxipotentiál értékeit. A 30 különböző standard redoxipotenciál kíváló korrelációt mutat a tiolát bázicitás mértékével, ez biztos alapot jelenthet egy hatásos és szelektív antioxidáns vegyület kifejlesztéséhez.

9. BIBLIOGRAPHY

1.   Villamena FA. Molecular basis of oxidative stress: chemistry, mechanisms, and disease pathogenesis. John Wiley & Sons, Hoboken, 2013: xvii.

2.   Nagy P. (2013) Kinetics and mechanisms of thiol-disulfide exchange covering direct substitution and thiol oxidation-mediated pathways. Antioxid Redox Sign, 18: 1623-1641.

3.   Cooper AJ. (1983) Biochemistry of sulfur-containing amino acids. Annu Rev Biochem, 52: 187-222.

4.   Marquet A, Tse Sum Bui A, Smith AG, Warren MJ. (2007) Iron-sulfur proteins as initiators of radical chemistry. Nat Prod Rep, 24: 1027-1040.

5.   Phillips RS, May SW. (1981) Enzymatic sulphur oxygenation reactions. Enzyme Microb Tech, 3: 9-18.

6.   Hutcherson RU, Broderick JB. (2012) Radical SAM enzymes in methylation and methylthiolation. Metallomics, 4: 1149-1154.

7.   Zou C-G, Banerjee R. (2005) Homocysteine and redox signaling. Antioxid Redox Sign, 7: 547-559.

8.   Ueland PM, Refsum H, Stabler SP, Malinow MR, Andersson A, Allen RH. (1993) Total homocysteine in plasma or serum: methods and clinical applications. Clin Chem, 39: 1764-1779.

9.   Gilbert HF. (1995) Thiol/disulfide exchange equilibria and disulfide bond stability. Method Enzymol, 251: 8-28.

10.   Zilmer M, Soomets U, Rehema A, Langel Ü. (2005) The glutathione system as an attractive therapeutic target. Drug Design Reviews Online, 2: 121-127.

11.   Sugamura K, Keaney Jr JF. (2011) Reactive oxygen species in cardiovascular disease. Free Rad Bio Med, 51: 978-992.

12. Head E. (2009) Oxidative damage and cognitive dysfunction: antioxidant treatments to promote healthy brain aging. Neurochem Res, 34: 670-678.

13. Kosower NS, Kosower EM. (1978) The glutathione status of cells. Int Rev Cytol, 54: 109-160.

14. Huxtable RJ. Biochemistry of Sulfur. Plenum Press, New York, 1986: 1-6.

15. Sies H. Oxidative Stress. Academic Press, New York, 1985: 1-7.

16. Keire DA, Strauss E, Guo W, Noszál B, Rabenstein DL. (1992) Kinetics and equilibria of thiol/disulfide interchange reactions of selected biological thiols and related molecules with oxidized glutathione. J Org Chem, 57: 123-127.

17. Rabenstein DL, Yeo PL. (1994) Kinetics and equilibria of the formation and reduction of the disulfide bonds in arginine vasopressin and oxytocin by thiol/disulfide interchange with glutathione and cysteine. J Org Chem, 59: 4223-4229.

18. Halliwell B. (2006) Oxidative stress and neurodegeneration: where are we now? J Neurochem, 97: 1634-1658.

19. Bachhawat AK, Thakur A, Kaur J, Zulkifli M. (2013) Glutathione transporters. BBA-Gen Subjects, 1830: 3154-3164.

20. Millis KK, Weaver KH, Rabenstein DL. (1993) Oxidation/reduction potential of glutathione. J Org Chem, 58: 4144-4146.

21. Pirie NW, Pinhey KG. (1929) The titration curve of glutathione. J Biol Chem, 84: 321-333.

22. Li NC, Gawron O, Bascuas G. (1954) Stability of zinc complexes with glutathione and oxidized glutathione. J Am Chem Soc, 76: 225-229.

23. Martin RB, Edsall JT. Glutathione: ionization in basic solutions and molecular rearrangement in strongly acid solutions. Bull Soc Chim Biol, 40: 1763-1771.

24. Pillai L, Boss RD, Greenberg MS. (1979) On the role of solvent in complexation equilibria. II. The acid-base chemistry of some sulfhydryl and ammonium-containing amino acids in water-acetonitrile mixed solvents. J Sol Chem, 8: 635-646.

25. Rabenstein DL. (1973) Nuclear magnetic resonance studies of the acid-base chemistry of amino acids and peptides. I. Microscopic ionization constants of glutathione and methylmercury-complexed glutathione. J Am Chem Soc, 95: 2797-2803.

26. Noszál B, Szakács Z. (2003) Microscopic protonation equilibria of oxidized glutathione. J Phys Chem B, 107: 5074-5080.

27. Kolthoff IM, Stricks W, Kapoor RC. (1955) Equilibrium constants of exchange reactions of cystine with glutathione and with thioglycolic acid both in the oxidized and reduced state. J Am Chem Soc, 77: 4733-4739.

28. Eldjarn L, Pihl A. (1957) The equilibrium constants and oxidation-reduction potentials of some thiol-disulfide systems. J Am Chem Soc, 79: 4589-4593.

29. Wilson JM, Bayer RJ, Hupe DJ. (1977) Structure-reactivity correlations for the thiol-disulfide interchange reaction. J Am Chem Soc, 99: 7922-7926.

30. Szajewski RP, Whitesides GM. (1980) Rate constants and equilibrium constants for thiol-disulfide interchange reactions involving oxidized glutathione. J Am Chem Soc, 102: 2011-2026.

31. Weaver KH, Rabenstein DL. (1995) Thiol/disulfide exchange reactions of ovothiol A with glutathione. J Org Chem, 60: 1904-1907.

32. Bjerrum N. (1923) Dissoziationskonstanten von mehrbasischen Säuren und Ihre Anwendung zur Berechnung molekularer Dimensionen. Z Physik Chem Stoechiom Verwandschaftsl, 106: 219-241.

33. Szakács Z, Kraszni M, Noszál B. (2004) Determination of microscopic acid-base parameters from NMR-pH titrations. Anal Bioanal Chem, 378: 1428-1448.

34. Palumbo A, d'Ichia M, Misuraca G, Prota G. (1982) Isolation and structure of a new sulphur-containing amino acid from sea urchin eggs. Tetrahedron Lett, 23: 3207-3208.

35. Palumbo A, Misuraca G, d'Ischia M, Donaudy F, Prota G. (1984) Isolation and distribution of 1-methyl-5-thiol-L-histidine disulphide and a related metabolite in eggs from echinoderms. Comp Biochem Physiol, 78B: 81-83.

36. Turner E, Somers CE, Shapiro B. (1985) The relationship between a novel NAD(P)H oxidase activity of ovoperoxidase and the CN⁻ resistant respiratory burst that follows fertilization of sea urchin eggs. J Biol Chem, 260: 13163-13171.

37. Turner E, Klevit R, Hager LJ, Shapiro BM. (1987) Ovothiols, a family of redox-active mercaptohistidine compounds from marine invertebrate eggs. Biochemistry, 26: 4028-4036.

38. Selman-Reimer S, Duhe RJ, Stockman BJ, Selman BR. (1991) L-1-N-methyl-4-mercaptohistidine disulfide, a potential endogenous regulator in the redox control of chloroplast coupling factor 1 in Dunaliella. J Biol Chem, 266: 182-188.

39. Turner E, Hager LJ, Shapiro BM. (1988) Ovothiol replaces glutathione peroxidase as a hydrogen peroxide scavenger in sea urchin eggs. Science, 242: 939-941.

40. Holler TP, Hopkins PB. (1990) Ovothiols as free-radical scavengers and the mechanism of ovothiol-promoted NAD(P)H-O2 oxidoreductase activity. Biochemistry, 29: 1953-1961.

41. Spies HSC, Steenkamp DJ. (1994) Thiols of intracellular pathogens: identification of ovothiol A in *Leishmania donovani* and structural analysis of a novel thiol from *Mycobacterium bovis*. Eur J Biochem, 224: 203-213.

42. Ariyanayagam MR, Fairlamb AH. (2001) Ovothiol and trypanothione as antioxidants in trypanosomatids. Mol Biochem Parasit, 115: 189-198.

43. Ondarza RN, Iturbe A, Hernández E, Hurtado G. (2002) Thiol compounds from a free-living pathogenic opportunistic amoeba, *Acanthamoeba polyphaga.* Biotechnol Appl Biochem, 36: 195-204.

44. Ondarza RN, Iturbe A, Hernández E, Hurtado G. (2003) Low-molecular-mass thiol compounds from a free-living highly pathogenic amoeba, *Naegleria fowleri.* Biotechnol Appl Biochem, 37: 195-204.

45. Krauth-Siegel RL, Leroux AE. (2012) Low-molecular-mass antioxidants in parasites. Antioxid Redox Sign, 17: 583-607.

46. Holler TP, Hopkins PB. (1988) Ovothiols as biological antioxidants. The thiol group of ovothiol and glutathione are chemically distinct. J Am Chem Soc, 110: 4837-4838.

47. Marjanovic B, Simic MG, Jovanovic SV. (1995) Heterocyclic thiols as antioxidants: why ovothiol C is a better antioxidant than ergothioneine. Free Radical Biol Med, 18: 679-685.

48. Bailly F, Zoete V, Vamecq J, Catteau JP, Bernier JL. (2000) Antioxidant actions of ovothiol-derived 4-mercaptoimidazoles: glutathione peroxidase activity and protection against peroxynitrite-induced damage. FEBS Lett, 486: 19-22.

49. Zoete V, Vezin H, Bailly F, Vergoten G, Catteau JP, Bernier JL. (2000) 4-Mercaptoimidazoles derived from the naturally occurring antioxidant ovothiols 2. Computaional and experimental approach of the radical scavenging mechanism. Free Radical Res, 32: 525-533.

50. Zoete V, Bailly F, Vezin H, Teissier E, Duriez P, Fruchart JC, Catteau JP, Bernier JL. (2000) 4-Mercaptoimidazoles derived from the narurally occurring antioxidant ovothiols 1. Antioxidant properties. Free Radical Res, 32: 515-524.

51. Zoete V, Bailly F, Catteau JP, Bernier JL. (1997) Design, synthesis and antioxidant properties of ovothiol-derived 4-mercaptoimidazoles. J Chem Soc Perkin Trans 1, 2983-2988.

52.   Bailly F, Azaroual N, Bernier JL. (2003) Design, synthesis and glutathione peroxidase-like properties of ovothiol-derived diselenides. Bioorg Med Chem, 11: 4623-4630.

53.   Vamecq J, Maurois P, Bac P, Bailly F, Bernier JL, Stables JP, Husson I, Gressens P. (2003) Potent mammalian cerebroprotection and neuronal cell death inhibition are afforded by a synthetic antioxidant analogue of marine invertebrate cell protectant ovothiols. Eur J Neurosci, 18: 1110-1120.

54.   Schmidt A, Krauth-Siege RL. (2002) Enzymes of the trypanothione metabolism as targets for antitrypanosomal drug development. Curr Top Med Chem, 2: 1239-1259.

55.   Steenkamp DJ. (2002) Thiol metabolism of the trypanosomatids as potential drug targets. Life, 53: 243-248.

56.   Jocelyn PC. Biochemistry of the SH group, Academic Press, New York, 1972.

57.   Tóth G, Baska F, Schretner A, Rácz Á, Noszál B. (2013) Species-specific basicities regulate molecular recognition in receptor binding in silico docking of thyroid hormones. Eur Biophys J, 42: 721-730.

58.   Ebert L. (1926) Zur Abschätzung der Zwitterionmenge in Ampholytlösungen. Z Phys Chem, 121: 385-400.

59.   Martin BR. (1961) A complete ionization scheme for citric acid. J Phys Chem, 65: 2053-2055.

60.   Santos MA, Esteves MA, Vaz MC, Frausto da Silva JJRF, Noszál B, Farkas E. (1997) Microscopic acid-base equilibria of a synthetic hydroxamate siderophore analog, piperazine-1,4-bis(N-methylacetohydroxamic acid). J Chem Soc Perkin Trans 2, 10: 1977-1983.

61.   Szakács Z, Hägele G, Tyka R. (2004) 1H/31P NMR pH indicator series to eliminate the glass electrode in NMR spectroscopic pKa determinations. Anal Chim Acta, 522: 247-258.

62.   Orgován G, Noszál B. (2011) Electrodeless, accurate pH determination in highly basic media using a new set of ^{1}H NMR pH indicators. J Pharm Biomed Anal, 54: 958-964.

63.   Vogl O, Rehman AU, Zarras P. (2000) Polycationic Salts V [1]. ^{15}N NMR spectra of amines, ammonium salt monomers, and polymers of styrene based trialkylammonium salts. Monatschefte für Chemie, 131: 437-449.

64.   Szakács Z, Noszál B. (1999) Protonation microequilibrium treatment of polybasic compounds with any possible symmetry. J Math Chem, 26: 139-155.

65.   Vanhamme L, van der Boogaart A, Van Huffel S. (1997) Improved method for accurate and efficient quantification of MRS data with use of prior knowledge. J Magn Reson, 129: 35-43.

66.   Naressi A, Couturier C, Devos JM, Janssen M, Mangeat C, de Beer R, Graveron-Demilly D. (2001) Java-based graphical user interface for the MRUI quantitation package. Magn Reson Mater Phys, 12: 141-152.

67.   Holler TP, Ruan F, Spaltenstein A, Hopkins PB. (1989) Total synthesis of marine mercaptohistidines: ovothiols A, B, and C. J Org Chem, 54: 4570-4575.

68.   Abdo M-R, Joseph P, Boigegrain R-A, Liautard J-P, Montero J-L, Köhler S, Winum J-Y. (2007) *Brucella suis* histidinol dehydrogenase: synthesis and inhibition of a series of substituted benzylic ketones derived from histidine. Bioorg Med Chem, 15: 4427-4433.

69.   Colombo R, Colombo F, Derome AE, Jones JH, Rathbone DL, Thomas DW. (1985) The differentiation of π- and τ-derivatised histidines. J Chem Soc Perkin Trans 1, 1811-1815.

70.   Zaramella S, Heinonen P, Yeheskiely E, Strömberg R. (2003) Facile determination of the protecting group location of N^{im}-protected histidine derivatives by ^{1}H-^{15}N heteronuclear correlation NMR. J Org Chem, 68: 7521-7523.

71.   Sudmeier JL, Reilly CN. (1964) Nuclear magnetic resonance studies of protonation of polyamine and aminocarboxylate compounds in aqueous solution. Anal Chem, 36: 1698–1706.

72.   Sayer TL, Rabenstein DL. (1976) Nuclear magnetic resonance studies of the acid-base chemistry of amino acids and peptides. III. Determination of the microscopic and macroscopic acid dissociation constants of a,w-diaminocarboxylic acids. Can J Chem, 54: 3392–3403.

73.   Noszál B, Guo W, Rabenstein DL. (1992) Characterization of the macroscopic and microscopic acidbase chemistry of the native disulfide and reduced dithiol forms of oxytocin, arginine-vasopressin, and related peptides. J Org Chem, 57: 2327–2334.

74.   Surprenant HL, Sarneski JE, Key RR, Byrd JT, Reilly CN. (1980) Carbon-13 NMR studies of amino acids: chemical shifts, protonation shifts, microscopic protonation behavior. J Magn Reson, 40: 231–243.

75.   Srinivasan U, Mieyal PA, Mieyal JJ. (1997) pH profiles indicative of rate-limiting nucleophilic displacement in thioltransferase catalysis. Biochemisty, 36: 3199-3206.

76.   Jao SC, Ospina SME, Berdis AJ, Starke DW, Post CB, Mieyal JJ. (2006) Computational and mutational analysis of human glutaredoxin (thioltransferase): Probing the molecular basis of the low pKa of cysteine 22 and its role in catalysis. Biochemistry, 45: 4785-4796.

10. PUBLICATIONS

10.1 Publications pertaining to the doctoral thesis

1.   **Mirzahosseini A**, Orgován G, Hosztafi S, Noszál B. (2014) The complete microspeciation of ovothiol A, the smallest octafarious antioxidant biomolecule. Anal Bioanal Chem, 406: 2377-2387.

2.   **Mirzahosseini A**, Noszál B. (2014) The species- and species-specific acid-base properties of biological thiols and their homodisulfides. J Pharm Biomed Anal, 95: 184-192.

3.   **Mirzahosseini A**, Szilvay A, Noszál B. (2014) The species- and species-specific acid-base properties of penicillamine and its homodisulfide. Chem Phys Lett, 610-611: 62-69.

4.   **Mirzahosseini A**, Hosztafi S, Tóth G, Noszál B. (2014) A cost-effective synthesis of enantiopure ovothiol A from L-histidine, its natural precursor. Arkivoc, 6: 1-9.

5.   **Mirzahosseini A**, Orgován G, Tóth G, Hosztafi S, Noszál B. (2015) The complete microspeciation of ovothiol A disulfide: a hexabasic symmetric biomolecule. J Pharm Biomed Anal, 107C: 209-216.

6.   **Mirzahosseini A**, Somlyay M, Noszál B. (2015) The comprehensive acid-base characterization of glutathione. Chem Phys Lett, 622: 50-56.

7.   **Mirzahosseini A**, Somlyay M, Noszál B. (2015) Species-specific thiol-disulfide equilibrium constants: a tool to characterize redox transitions of biological importance. J Phys Chem B, 119: 10191-10197.

8.   **Mirzahosseini A**, Noszál B. (2016) Species-specific thiol-disulfide equilibrium constants of ovothiol A and penicillamine with glutathione. RSC Advances, 6: 26757-26764.

9.   **Mirzahosseini A**, Szilvay A, Noszál B. (2016) Physico-chemical profiling of α-lipoic acid and related compounds. Chem Biodivers, 13: 861-869.

10.   **Mirzahosseini A**, Noszál B. (2016) Species-specific standard redox pontential of thiol-disulfide systems: a key parameter to develop agents against oxidative stress. Scientific Reports, 6: 37596.

10.2 Publications pertaining to different subjects

1.   **Mirzahosseini A**, Dalmadi B, Csutora P. (2013) Histamine receptor H4 regulates mast cell degranulation and IgE induced FcεRI upregulation in murine bone marrow-derived mast cells. Cell Immunol, 283: 38-44.

2.   **Mirzahosseini A**, Kovács M, Kánai K, Csutora P, Dalmadi B. (2014) BODIPY® FL histamine as a new modality for quantitative detection of histamine receptor upregulation upon IgE sensitization in murine bone marrow-derived mast cells. Cytometry Part A, 87: 23-31.

3.   Fiedler GB, Meyerspeer M, Schmid AI, Goluch S, Schewzow K, Laister E, **Mirzahosseini A**, Niess F, Unger E, Woltz M, Moser E. (2015) Localized semi-LASER dynamic 31P magnetic resonance spectroscopy of the soleus during and following exercise at 7 T. Magn Reson Mater Phy, 28: 493-501.

4.   Budai KA, **Mirzahosseini A**, Noszál B, Tóth G. (2015) Az elhízás gyógyszeres kezelése – The pharmacotherapy of obesity [in Hungarian]. Acta Pharm Hung, 85: 3-17.

5.   Fiedler GB, Schmid AI, Goluch S, Schewzow K, Laister E, Niess F, Unger E, Woltz M, **Mirzahosseini A**, Kemp GJ, Moser E, Meyerspeer M. (2016) Skeletal muscle ATP synthesis and cellular H^+ handling measured by localized ^{31}P-MRS during exercise and recovery. Scientific Reports, 6:32037.

ACKNOWLEDGEMENT